Climate impact on mean annual cycle and interannual variability of CO₂ fluxes in European DBF and ENF forests: insights from observations and state-of-the-art data-driven and process-based models

Asmat Ullah[1], Julien Crétat[1], Gaïa Michel[1,2], Olivier Mathieu[1], Mathieu Thevenot[1], Andrey Dara[3], Robert Granat[3], Zhendong Wu[4,5], Clément Bonnefoy-Claudet[1], Julianne Capelle[1], Jean Cacot[6], John S. Kimball[7]

[1] Biogéosciences, UMR 6282 CNRS, Université Bourgogne Europe, Dijon, France
[2] AgroParisTech, 91120, Palaiseau, France
[3] CarbonSpace Ltd., D04H1F3 Dublin, Ireland
[4] Department of Physical Geography and Ecosystem Science, Lund University, Lund, Sweden
[5] ICOS ERIC, Carbon Portal, Lund, Sweden
[6] Bibracte, Glux-en-Glenne, France
[7] Numerical Terradynamic Simulation Group, University of Montana, Missoula, MT, United States of America

Correspondence to: Julien Crétat (julien.cretat@ube.fr)

Abstract.

The impact of climate on the annual cycle and interannual variability of CO_2 fluxes is assessed in European evergreen needleleaf (ENF) and deciduous broadleaf (DBF) forests using observations from 19 sites alongside process-based and data-driven model outputs. We first evaluate the models' ability to reproduce observed patterns before using them as complementary tools to investigate climate influences. All models capture the temporal phasing of CO_2 fluxes, including the shorter CO_2 sequestration period in northern than southern Europe, the more pronounced annual cycle for DBFs than ENFs in central Europe, and strong interannual variability across all sites. However, they struggle to accurately reproduce the magnitude of observed fluxes, generally underestimating both sequestration strength and interannual variability. Across all datasets, CO_2 sequestration is favored under relatively hot and dry conditions from late spring to early fall. The coupling between climate and CO_2 fluxes is, however, stronger in northern and central Europe than in southern Europe, where climate seasonality is less pronounced. At the interannual timescale, the climate impact on observed CO_2 fluxes appears spatially noisy due to limited temporal coverage and differences in data availability across sites. Despite uncertainties, the models provide a clearer picture of climate influences, revealing spatial and seasonal variations. Atmospheric factors (i.e., 2 m temperature and vapor pressure deficit) primarily drive interannual CO_2 flux variability in northern and central Europe, whereas soil moisture plays a dominant role in southern Europe. Winter and fall CO_2 release increases with elevated temperature and VPD in northern and central Europe but under low VPD in southern Europe. In northern and central Europe, CO_2 sequestration is enhanced by anomalously hot and dry conditions in spring, while by anomalously cold and wet conditions in summer. In southern Europe, CO_2 sequestration is also favored by anomalously cold and wet conditions from May to September.

Key words: Net ecosystem exchange, gross primary production, ecosystem respiration, climate, annual cycle, interannual variability, DBF, ENF

1 Introduction

Forest ecosystems are the largest part of the land CO_2 sink (Lindeskog et al., 2021), with up to 20-50% of anthropogenic CO_2 emissions (land-use changes excluded) sequestered for the 2000-2010 period (Le Quéré et al., 2018; Pugh et al., 2019; Pan et al., 2024). In Europe, recent estimations suggest a slight increase in CO_2 sequestration by forest ecosystems over the 2000-2021 period mainly due to the fertilization effect of increased atmospheric CO_2 concentration (Prentice et al., 2001; Piao et al., 2009; Schimel et al., 2015; Walker et al., 2020; Sitch et al., 2024). This trend remains, however, weak, because the fertilization effect has almost been compensated by a decrease in CO_2 sequestration induced by climate change (Sitch et al., 2024). The extent to which climate controls CO_2 flux exchanges between the atmosphere and European forest ecosystems is thus a burning question in the context of climate change.

Numerous studies have demonstrated the strong influence of climate on CO_2 exchanges between the atmosphere and forest ecosystems. The annual cycle, and to a lesser extent, interannual variability of these fluxes, are driven by factors such as incident shortwave radiation, temperature, atmospheric evaporative demand, and the water cycle, including soil moisture dynamics (Haszpra et al., 2005; Tang et al., 2014; von Buttlar et al., 2018; Kong et al., 2022; Sharma et al., 2022; Li et al., 2023; Xu et al., 2023). The dominant climate factor influencing CO_2 fluxes depends on the specific component considered. The variability in net ecosystem exchanges (NEE) is a mixed response of its two components: gross primary production (GPP), which sequesters CO_2 into the ecosystem through photosynthesis, and ecosystem respiration (RECO), which releases CO_2 into the atmosphere from forest metabolism (autotroph respiration) and the decomposition of organic matter by fungi and bacteria (heterotrophic respiration). GPP is primarily driven by vapour pressure deficit (VPD), shortwave radiation, temperature, and soil moisture, while RECO is mainly influenced by precipitation, soil moisture, and temperature (Messori et al., 2019).

The influence of climate on CO_2 fluxes also depends on several additional factors, with seasonality playing a crucial role. Severe heat waves and droughts acted to reduce CO_2 sequestration in summer at the Europe-wide scale in 2003 (Ciais et al., 2005), in northern Europe in 2018 (Smith et al., 2020; Thompson et al., 2020) and in central and southeastern Europe in 2022 (van der Woude et al., 2023). On the other hand, anomalously high temperature under normal soil moisture conditions in spring set favourable growth conditions, hence increased CO_2 sequestration, such as in northern Europe in 2018 (Smith et al., 2020). The climatic zone under consideration is also a key factor. For instance, GPP is mostly influenced by soil moisture in the Mediterranean region, VPD over parts of central Europe and temperature over Scandinavia, parts of eastern and south-eastern Europe and higher elevations (Seddon et al., 2016; Madani et al., 2017). The influence of climate on CO_2 flux exchanges is further shaped by various factors, including soil properties (Kurbatova et al., 2008; Besnard et al., 2018; Curtis and Gough, 2018; Martinez del Castillo et al., 2022), forest management practices (Carrara et al., 2003; Saunders et al., 2012), tree age (Kurbatova et al., 2008; Besnard et al., 2018) and tree species (Carrara et al., 2003; Carrara et al., 2004; Welp et al., 2007; Kong et al., 2022).

Assessing the impact of climate on CO_2 flux exchanges remains challenging. The main reason involves the scarcity of multi-year CO_2 fluxes measured by eddy covariance above the canopy (Burba, 2021). At the European scale,

the Integrated Carbon Observation System (ICOS) network provides standardized and open data from 98 ecosystem stations across 16 countries. The flux tower measurements remain limited in number and temporal depth and unevenly distributed spatially, making it difficult to assess the impact of climate on the interannual variability (and trend)s in CO_2 flux exchanges and to map them. Process-based and data-driven models allow us to tackle the above limitations. Process-based models, such as dynamical vegetation models, are routinely used to assess CO_2 flux exchanges between the atmosphere and the biosphere (Friedlingstein et al., 2023). These are mechanistic models (Friedlingstein et al., 2006; Sitch et al., 2008) allowing for testing the response of CO_2 fluxes to individual and combined forcing (Sitch et al., 2024). Data-driven models rely on the identification of statistical relationships between flux tower measures by eddy-covariance and corresponding land use, vegetation properties and climate characteristics. Based on these statistical relationships, empirical models are built and used for upscaling, i.e., for assessing CO_2 fluxes in regions where they are not measured (Tramontana et al., 2016; Jung et al., 2019; Jung et al., 2020; Zhuravlev et al., 2022). Both approaches have limitations. Estimations of CO_2 flux exchanges are highly sensitive to physical parameterizations (Cai and Prentice, 2020) and atmospheric forcing (Wu et al., 2017; Hardouin et al., 2022) in process-based models. The reliability of data-driven models is limited by the sparse and uneven distribution of flux tower measurements and by the underlying statistical methods used to build them (Jung et al., 2020). While not perfect, process-based and data-driven models provide satisfactory results for capturing large-scale patterns compared to e.g. satellite estimations (Wang et al., 2023). This makes them valuable complementary tools to observational data.

Most recent studies examining the influence of climate on the temporal dynamics of European forest CO_2 fluxes rely on case studies and primarily focus on spring and summer conditions (Smith et al., 2020; Thompson et al., 2020; van der Woude et al., 2023). However, a more comprehensive assessment is needed across the entire annual cycle, as CO_2 release during fall and winter is expected to increase under climate change. Additionally, climate conditions vary significantly between northern and southern Europe, necessitating a broader spatial perspective. These objectives are addressed at the monthly timescale, which is considered sufficiently fine to capture both the CO_2 flux annual cycle and its interannual variability.

This study addresses these gaps by investigating the impact of climate on both the annual cycle and interannual variability of CO_2 fluxes in European evergreen needleleaf (ENF) and deciduous broadleaf forests (DBF). Using ICOS network observations alongside state-of-the-art data-driven and process-based model estimates, we first characterize the observed annual cycle and interannual variability of CO_2 fluxes across Europe. We then evaluate model performance in capturing the temporal phasing and magnitude of these fluxes at the site scale. Finally, we assess the influence of climate on both seasonal and interannual CO_2 flux variations, leveraging the extended temporal coverage provided by models.

2 Materials & Methods

2.1 Site description

163 Out of the 24 ENF and DBF sites from the ICOS network, we selected the 19 sites (Fig. 1), 13 classified as ENF

164 and 6 as DBF, for which observed CO_2 fluxes are available for at least 5 years (Table 1). These sites allow to

165 sample the different climatic zones of Europe. Three ENF sites (FR-Bil, FR-FBn and IT-SR2) are located in the

166 northern region of southern Europe, close to 45°N, and ranging from sea level to 400 m in elevation. They are

167 characterized by mild, wet winters and hot dry summers, with annual mean temperature and precipitation of 12.9–

168 13.90 °C and 700–960 mm, respectively. Four ENF sites (FI-Hyy, FI-Let, SE-Nor and SE-Svb) are located in

169 northern Europe (60-65°N) at an elevation below 270 m. They are characterized by subarctic climate with annual

170 mean temperature and precipitation of 1.8–6.5 °C and 586–711 mm, respectively. The remaining twelve sites (6

171 DBFs and 6 ENFs) are situated in central Europe within the 45–60°N, 2.5–20°E domain, encompassing a wide

172 range of elevations (40–1730 m) and spanning temperate to continental climates. As a result, they exhibit

173 substantial variability in annual mean temperature (4.3–11.4 °C) and precipitation (563–1338 mm).

174
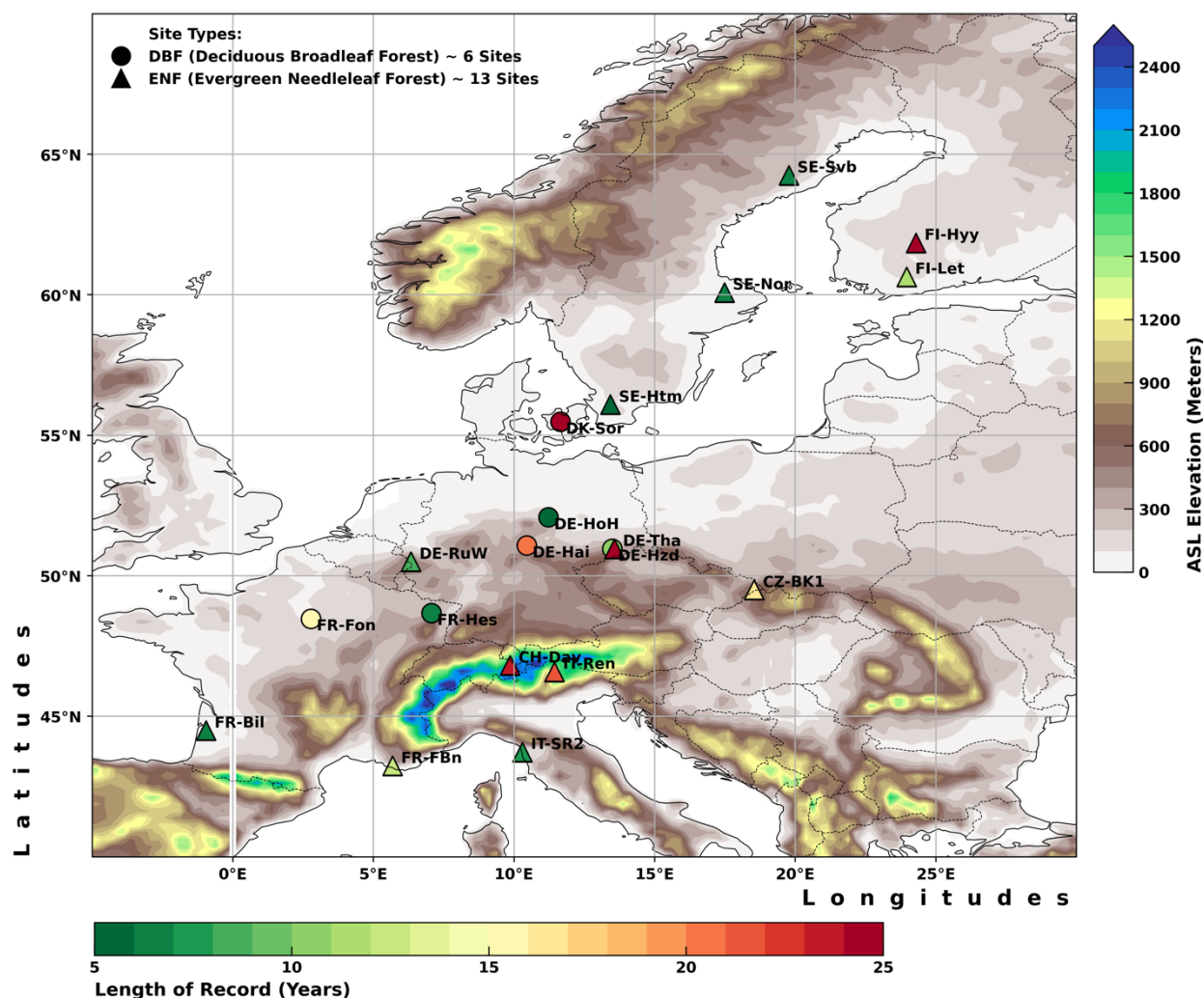
175
176 **Figure 1.** Location of the CO_2 flux measurement sites from the FLUXNET network across Europe selected for
177 this study. The symbol "●" corresponds to the 6 sites located in Deciduous Broadleaf Forest (DBF) while the
178 symbol "▲" indicates the 13 sites located in the Evergreen Needleleaf Forests (ENF). The vertical colour scale
179 represents the terrain height (ASL) in meters. The horizontal colour scale indicates the length of the CO_2 flux
180 record for each site. The elevation layer comes from National Geophysical Data Center/NESDIS/NOAA/U.S.
181 Department of Commerce (1995): TerrainBase, Global 5 Arc-minute Ocean Depth and Land Elevation from the
182 US National Geophysical Data Center (NGDC), https://doi.org/10.5065/E08M-4482. Distributed under CC by 4.0.

Table 1. European FLUXNET sites examined in this study.

Site Name	Site ID	Latitude (°North)	Longitude (°East)	Elevation (Meters)	Land cover	Period of record	Length of record (Years)	MAT (°C)	MAP (mm)
Northern Europe (Above 60°N)									
Svartberget	SE-Svb	64.25611	19.7745	267	ENF	2014/01 – 2020/12	7	1.8	614.0
Hyytiala	FI-Hyy	61.8474	24.2948	181	ENF	1996/01 – 2020/12	25	3.5	711.0
Lettosuo	FI-Let	60.6418	23.9595	111	ENF	2009/01 – 2020/12	12	4.6	627.0
Norunda	SE-Nor	60.0865	17.4795	45	ENF	2014/01 – 2020/12	7	6.5	586.0
Central Europe (45°N – 60°N)									
Hyltemossa	SE-Htm	56.09763	13.41897	115	ENF	2015/01 – 2020/12	6	7.4	707.0
Soroe	DK-Sor	55.4859	11.6446	40	DBF	1996/01 – 2020/12	25	9.0	640.0
Hohes Holz	DE-HoH	52.08656	11.22235	193	DBF	2015/01 – 2020/12	6	9.1	563.0
Hainich	DE-Hai	51.0792	10.4522	430	DBF	2000/01 – 2020/12	21	8.3	744.0
Hetzdorf	DE-Hzd	50.96381	13.48978	395	DBF	2010/01 – 2020/12	11	7.6	877.0
Tharandt	DE-Tha	50.9626	13.5651	385	ENF	1996/01 – 2020/12	25	8.1	829.0
Wustebach	DE-RuW	50.50493	6.330962	610	ENF	2012/01 – 2020/12	9	7.5	1250.0
Bily Kriz	CZ-BK1	49.5021	18.5369	875	ENF	2004/01 – 2020/12	17	6.2	1338.1
Hesse	FR-Hes	48.6741	7.06465	310	DBF	2014/01 – 2020/12	7	10.0	889.0
Fontainebleau-Barbeau	FR-Fon	48.4764	2.7801	103	DBF	2005/01 – 2020/12	16	11.4	678.9
Davos	CH-Dav	46.8153	9.8559	1639	ENF	1997/01 – 2020/12	24	4.3	876.0
Renon	IT-Ren	46.5869	11.4337	1730	ENF	1991/01 – 2020/12	22	4.9	970.8
Southern Europe (Below 45°N)									
Bilos	FR-Bil	44.49365	– 0.95609	39	ENF	2014/01 – 2020/12	7	12.9	960.1
San Rossore 2	IT-SR2	43.732	10.2909	4	ENF	2013/01 – 2020/12	8	15.3	950.0
Font-Blanche	FR-FBn	43.24079	5.67865	436	ENF	2008/01 – 2020/12	13	13.9	700.0

Columns 1–5 provide information on the site, including its name, ID, latitude, longitude, and elevation. Columns 6–8 describe the land cover classification, the period of available records, and the record length for each FLUXNET site. Columns 9–10 present the site's mean annual climatic characteristics, including temperature (MAT) and precipitation (MAP).

2.2 Carbon flux data

2.2.1 Observations

Measured CO_2 fluxes come from the Warm Winter 2020 (Team and Centre, 2022), an update of the FLUXNET2015 dataset (Pastorello et al., 2020) available on the ICOS platform (https://www.icos-cp.eu/data-products). For each site, we selected daily time series of NEE (NEE_VUT_REF), GPP (GPP_DT_VUT_REF) and RECO (RECO_DT_VUT_REF), the latter two fluxes being derived from the daytime flux partitioning method (Lasslop et al., 2010). Preliminary analyses show weak impact of the partitioning method (not shown).

198 The temporal coverage of the data varies by site (Table 1): less than 10 years for eight sites (SE-Svb, SE-Nor, SE-
199 Htm, DE-HoH, DE-RuW, FR-Hes, FR-Bil, and IT-SR2), between 10 and 20 years for five sites (FI-Let, DE-Hzd,
200 CZ-BK1, FR-Fon, and FR-FBn), and more than 20 years for six sites (FI-Hyy, DK-Sor, DE-Hai, DE-Tha, CH-
201 Dav, and IT-Ren). Given these limitations, the observational dataset likely lacks sufficient temporal depth to
202 robustly assess the impact of climate on tower CO_2 flux interannual variability, highlighting the usefulness of
203 models as complementary tools.

204

205 **2.2.2 Data-driven models**
206

207 Four data-driven models are used in this study (Table 2). The first data-driven model has been developed by the
208 CarbonSpace company. The CarbonSpace model is designed to quantify carbon exchange at the site-scale by
209 integrating remote sensing data, meteorological variables, and eddy-covariance flux measurements. A lagrangian
210 particle dispersion model is used for footprint gas attribution. A machine learning model is used to solve the non-
211 linear regression problem of estimating fluxes from remote sensing and meteorological variables (Zhuravlev et al.,
212 2022). For this study, the learning method was updated from the kernel method used in Zhuravlev et al. (2022) to
213 an ensemble tree method (Chen and Guestrin, 2016). The key advantages of the Carbon Space model include its
214 scalability, high spatial resolution, and improved prediction accuracy through robust data quality control and
215 advanced machine learning techniques. Carbon Space provides monthly NEE only but at a very high spatial
216 resolution (few hectares) from 01-2000 to 08-2023. This allows to get as close as possible to the 19 sites (around
217 1.8 ha centered on each tower) and their associated CO_2 flux measurement footprints.

218

219 The second and third data-driven models come from the FLUXCOM initiative (Tramontana et al., 2016; Jung et
220 al., 2019; Jung et al., 2020) and have been retrieved from the data portal of the Max Planck Institute for
221 Biochemistry (https://www.bgc-jena.mpg.de). The FLUXCOM models use eddy-covariance data from 224 flux-
222 tower sites from the FLUXNET La Thuile dataset (http://fluxnet.fluxdata. org/data/la-thuile-dataset/) and the
223 CarboAfrica network (Valentini et al., 2014). Among the various models available, we retained two models: a 3-
224 member ensemble forced by both ERA5 reanalysis (Hersbach et al., 2020) and satellite data from the Moderate
225 Resolution Imaging Spectroradiometer (MODIS) and a 9-member ensemble forced by MODIS only. The members
226 differ by the machine learning method used to build each of the two models detailed in Jung et al. (2019). These
227 models, named FLUXCOM-ERA5 and FLUXCOM-MODIS hereafter, provide global maps of monthly NEE, GPP
228 and RECO derived with a daytime partitioning. The FLUXCOM-ERA5 model has a coarser resolution (0.5° x
229 0.5°) than the FLUXCOM-MODIS (0.08° x 0.08°) but covers a longer period (1979-2018 versus 2001–2015).

230

231

232

233

234

235

236

237

238

Table 2. Data-driven and process-based models used in this study.

Type and Name of the Dataset	Ensemble Members	Temporal and Spatial Resolution	Temporal Coverage Available	Description	References
Data-driven models					
CarbonSpace	1	Monthly ~ Hectometric	01/2000 – 08/2023	Data-driven models trained using FLUXNET observations	Zhuravlev et al., (2022)
FLUXCOM-ERA5	3	Monthly / ~ 50 km	01/1979 – 12/2018		Jung et al. (2019, 2020); Tramontana et al. (2016)
FLUXCOM-MODIS	9	Monthly / 0.08° (~8 km)	01/2001 – 12/2015		Jung et al. (2019, 2020)
FLUXCOM-X-BASE	1	Monthly / 0.05° (~5 km)	01/2001 – 12/2021		Nelson et al. (2024)
Process-based models					
SMAP-L4C	1	Daily / ~ 9 km	03/2015 – 09/2023	Reanalysis assimilated satellite-derived soil moisture	Jones et al. (2017); Kimball et al. (2022)
TRENDY	15	Monthly / 0.5° and coarser depending on the model	Since 1700	Dynamic Global Vegetation Models (S3 simulation forced by time-varying CO_2, climate and land use observations	Friedlingstein et al. (2023); Sitch et al. (2024)

Column 1 specifies the model type and name. Columns 2–4 detail the number of members in each dataset, the space-time resolution, and the period of output availability. Columns 5–6 provide a brief description of each dataset along with references.

The fourth data-driven model, X-BASE, also comes from the FLUXCOM initiative (FLUXCOM-X hereafter, Nelson et al., 2024). This model uses qualitatively similar predictors as the previous generation of FLUXCOM models but incorporates more sites (294), improves the coverage and quality of the training, as well as satellite data processing, and resolves the diurnal cycle. Unlike the previous generation, one unique member is available (based on gradient-boosted regression trees) but at much higher spatial resolution (0.05° x 0.05°) and for a longer period (2001–2020).

The four data-driven models include most, if not all, ICOS sites mobilised in this study. They accurately capture the mean annual and seasonal cycles of CO_2 fluxes (Tramontana et al., 2016; Jung et al., 2020; He et al., 2022; Zhuravlev et al., 2022) and are expected to outperform process-based models since the latter do not assimilate observed CO_2 fluxes. The methodological framework (e.g., machine learning model, forcing data and horizontal resolution) remains different between the data-driven models. An inter-model convergence will be interpreted as a forced response imposed by the observations. A divergence will be interpreted as uncertainties induced by the methodological framework.

2.2.3 Process-based models

Two process-based models are considered (Table 2): the SMAP (Soil Moisture Active Passive) Level 4 Carbon model (SMAP-L4C hereafter) and an ensemble of Dynamic Global Vegetation Models (DGVM) from the TRENDY project (https://sites.exeter.ac.uk/trendy). The SMAP-L4C product is produced operationally by the

NASA SMAP mission. It can be considered as a reanalysis product since it uses the Goddard Earth Observing System version 5 (GEOS-5) land model to assimilate SMAP L-band microwave observations and is forced with observed land cover and vegetation from the Moderate Resolution Imaging Spectroradiometer (MODIS) and Visible Infrared Imaging Radiometer Suite (VIIRS). The global processing is conducted on 1 km sub-grids using spatially aggregated MODIS PFTs and VIIRS fPAR inputs, allowing to distinguish up to eight individual plant functional types (PFTs) within each 9 km × 9 km product grid cell. However, the model processing uses coarser spatial resolution (9 km and 0.25 degree) daily inputs from the SMAP L4 soil moisture (L4_SM) and GMAO Forward Processor (FP) surface meteorology. Among other variables, the SMAP-L4C outputs provide daily NEE and GPP (RECO deduced from the difference between NEE and GPP) in a consistent global grid from March 2015 to September 2023 for each PFT, including DBFs and ENFs (Jones et al., 2017; Kimball et al., 2022). The 1-km PFT subclass distinction allows the differentiation of ENF and DBF. The L4C product is derived using coupled photosynthetic light-use efficiency and soil organic matter decomposition models to estimate daily NEE and its component carbon fluxes, where GPP is reduced from PFT-specific optimal rates for unfavourable daily climate conditions, including cold temperatures, low light levels, excessive atmospheric vapour pressure deficits and low root zone (0-1m depth) soil moisture levels defined from SMAP L4_SM and GMAO FP meteorology. The associated product quality assessment report gives details of the model algorithms and the calibration, validation, and performance of the L4C version 7 product used in this study (Endsley et al., 2023).

In addition to SMAP-L4C, this study also uses outputs from 15 Dynamic Global Vegetation Models (DGVMs) of the Trends and Drivers of Regional-Scale Terrestrial Sources and Sinks of Carbon Dioxide (TRENDY version 12) project. These models are routinely mobilised to assess global carbon budget trends and for attributing changes to CO_2, climate and land use (Friedlingstein et al., 2023; Sitch et al., 2024). Appendix Table 1 provides the list of the 15 DVGMs used in this study. Here, we used outputs from the S3 scenario, with simulations starting in 1700 and forced by time-varying observed CO_2, climate and land use change. All simulations have horizontal resolution of 0.5° x 0.5° and monthly outputs.

2.2.4 Climate data

To investigate the impact of climate on CO_2 fluxes, we use the ERA5-Land dataset (Muñoz-Sabater et al., 2019) produced by the European Centre for Medium-Range Weather Forecasts (ECMWF). This dataset results from the ECMWF land surface model (HTESSEL) operating at 0.1° spatial resolution and forced by the ERA5 reanalysis (Hersbach et al., 2020). This product provides hourly outputs for land surface, hydrological and meteorological variables from 1950 onwards. In this study, we use incident shortwave radiation, temperature at 2 m (T_{2m}) and averaged soil moisture (SM_{AVG}). We use the average of the four ERA5-Land soil moisture layers (0–7 cm, 7–28 cm, 28–100 cm, and 100–289 cm), representing the volumetric soil water content at different depths. Results obtained with incident shortwave radiation and T_{2m} lead to similar results. We therefore show the results for T_{2m} only. We also use relative humidity together with T_{2m} to compute the air vapour pressure deficit (VPD), an integrative metric accounting for both heat and water stress effects (Carrara et al., 2004; von Buttlar et al., 2018; Kong et al., 2022; van der Woude et al., 2023). The VPD is defined as the difference between the amount of

moisture that is actually in the air and the amount of moisture that air could hold at saturation. The VPD is computed using the Tetens formula (Monteith and Unsworth, 2007) following Eq. (1):

$$VPD = \left(1 - \frac{HU}{100}\right) * saturation\ vapor\ pressure = \left(1 - \frac{HU}{100}\right)\left(610.78 * \exp\left(\frac{T}{T+237.3} * 17.2694\right)\right) \quad (1)$$

In the end, three ERA5-Land climate variables (T_{2m}, SM_{AVG} and VPD) are used to assess the impact of climate on the annual cycle and interannual variability of CO_2 fluxes. These variables capture the influence of thermal, hydrological, and atmospheric moisture demand conditions on CO_2 flux dynamics.

2.3 Methodology

For the gridded datasets (ERA5-Land, FLUXCOM, TRENDY, and SMAP-L4C), we extracted the nearest grid point to each flux tower site. Note that SMAP-L4C simulates spurious CO_2 fluxes at the DE-Hzd site. Therefore, this site is not included in the analysis for this model. Since these datasets have varying temporal resolutions (Tables 1 and 2), all were aggregated to a monthly timescale. From these monthly values, we computed the mean annual cycle by averaging all available years in each dataset, along with interannual variability, defined by the standard deviation and coefficient of variation.

Model skill in capturing observed CO_2 flux variability is evaluated over overlapping periods between each model and observation. The number of overlapping years varies significantly across model–observation pairs (Fig. 2a). Magnitude and co-variability errors are assessed using bias and the Bravais-Pearson correlation coefficient (R), respectively. For the annual cycle, we computed monthly biases for each overlapping year and present the mean bias averaged across all months and years. Model skill in reproducing the seasonal timing of CO_2 fluxes is assessed by correlating the 12 monthly modelled and observed values within each overlapping year, with the multi-year mean R reported. Correlations are considered significant at the 95% confidence level if the mean p-value is below 0.05. For interannual variability, biases are calculated as the difference between modelled and observed standard deviations for each month. Co-variability between observed and modelled CO_2 fluxes is assessed only for model-observation pairs with at least 10 overlapping years, ensuring robust signal detection. Correlations were deemed significant when p < 0.05.

The impact of climate on CO_2 fluxes is assessed for overlapping years between each CO_2 flux dataset and ERA5-Land. The number of overlapping years varies widely across datasets (Fig. 2b), ranging from low coverage in observations and SMAP-L4C to over 70 years in TRENDY. The correlation coefficient (R) was used to assess climate impacts, with the mean R reported for the annual cycle and individual R values for interannual variability. To ensure results were not driven by long-term trends, analyses have been conducted using both raw and detrended climate time series (not shown), yielding similar outcomes. Additionally, for observed CO_2 fluxes, we verified ERA5-Land climate data reliability by comparing results with observed climate measurements from the FLUXNET database (not shown).

For conciseness, we primarily present results using the ensemble mean of FLUXCOM (ERA5 and MODIS) and TRENDY models. However, uncertainties arising from machine learning methods and DVGM physical parameterizations are discussed in the model evaluation section.
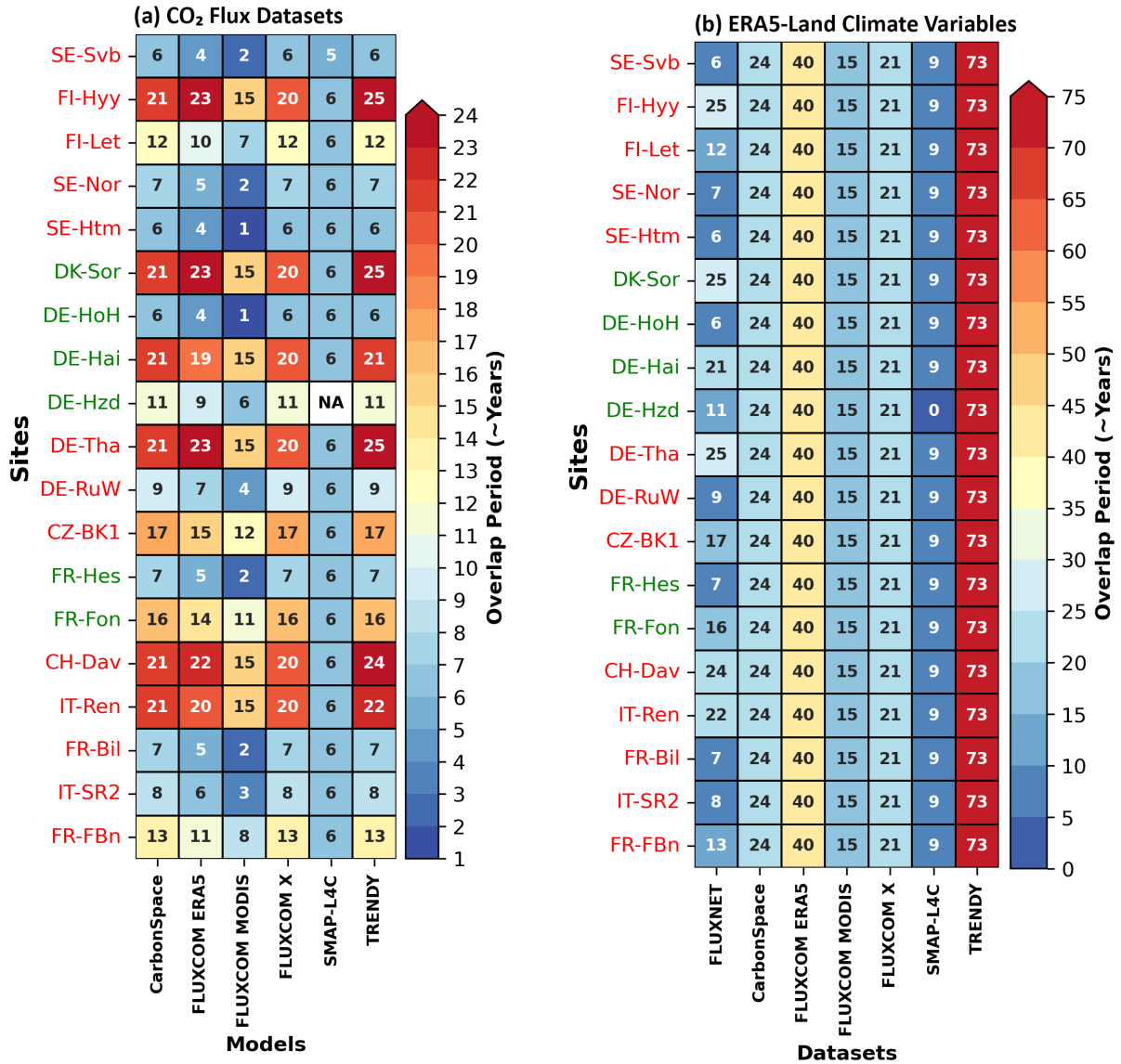
Figure 2. Number of overlapping years between **(a)** observed and modelled CO_2 fluxes, and **(b)** ERA5-Land climate and observed and modelled CO_2 fluxes. The overlapping periods in panel (a) are used to assess the model's ability to capture the annual cycle and interannual variability of CO_2 fluxes. In panel (b), the overlapping periods are used to evaluate the co-variability between CO_2 fluxes and the annual cycle and interannual variability of ERA5-Land climate.

3 Results

3.1 Observed climate and CO₂ fluxes mean annual cycle and interannual variability
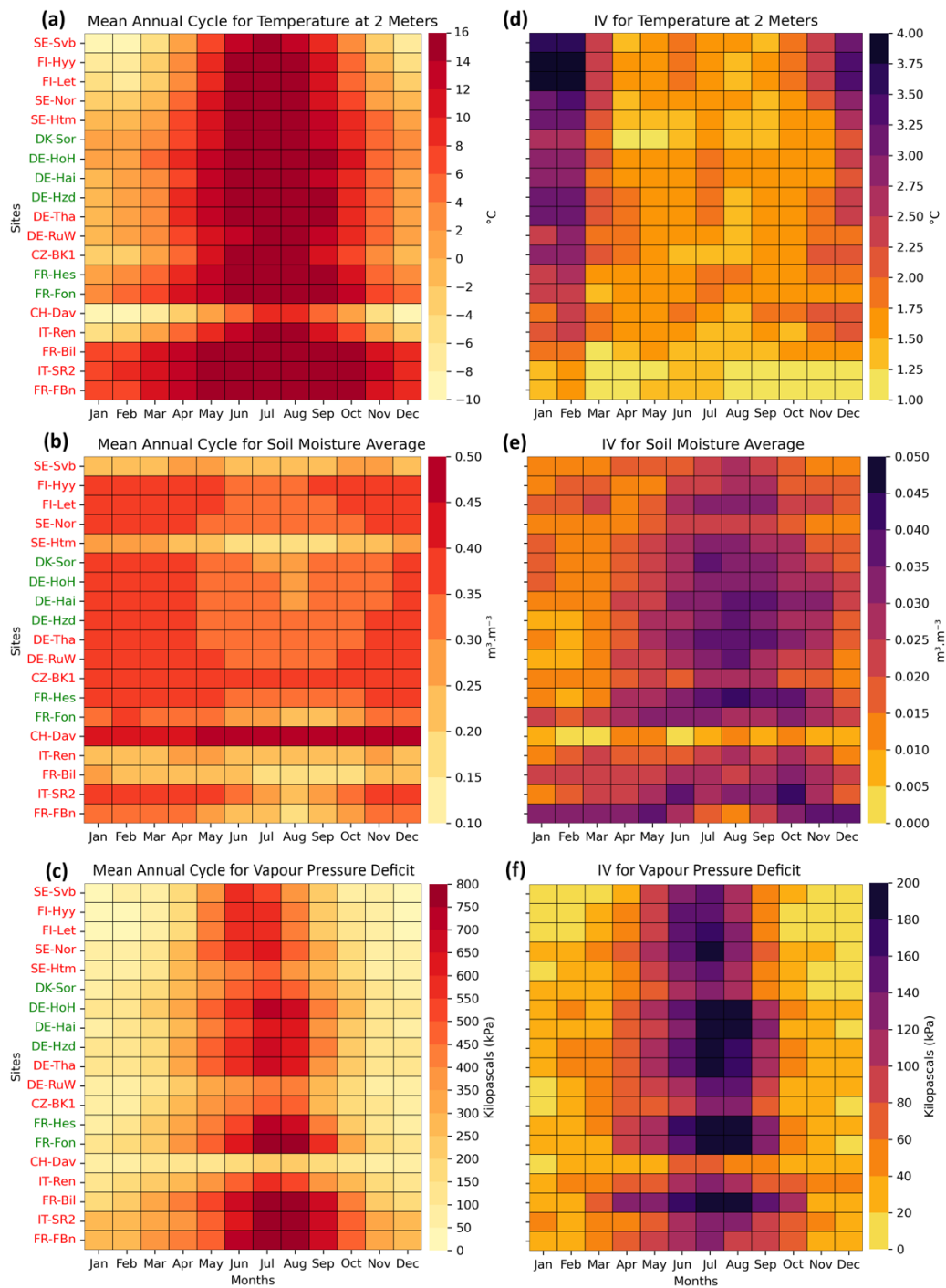
Figure 3. (a-c) Mean annual cycle and **(d-f)** interannual variability in monthly 2 m air temperature (T_{2m}), soil moisture (SM_{AVG}), and vapour pressure deficit (VPD), respectively, for each study site for the 1979–2023 period. Climate conditions at each site are extracted from the nearest grid point of the 9 km × 9 km ERA5-Land product. ENF sites are displayed in red text, while DBF sites are highlighted in green. Sites are ordered from north to south based on their latitude.

366   Figure 3 shows the mean annual cycle and interannual variability of T_{2m}, SM_{AVG} and VPD associated with each
367   site. Overall, all sites depict higher T_{2m} and VPD and lower SM in summer than in winter (Figs. 3a-c). A south-
368   north gradient is evident, with more marked annual amplitude and shorter summer in northern than southern
369   Europe. Few sites deviate from this pattern, including e.g., the Alpine site (CH-Dav), which depicts relatively cold
370   and wet conditions, as well as low VPD, all year long. While the interannual variability of T_{2m} is the largest in
371   winter regardless of the site, it significantly increases from south to north (Fig. 3d). The reverse is found for VPD,
372   with higher interannual variability in summer than winter, especially south of 60°N (Fig. 3f). The interannual
373   variability in SM_{AVG} (Fig. 3e) is low all year long in the Alpine site, relatively low in northern Europe, high from
374   spring to summer in the mid-latitudes and in fall and winter in the Mediterranean region (FR-FBn). Interestingly,
375   the pattern of SM_{AVG} interannual variability significantly differs from that of VPD, suggesting soil moisture
376   variability to be much more driven by precipitation than evapotranspiration variability.

377

378   Figure 4a displays the mean annual cycle of monthly NEE, GPP and RECO as provided by FLUXNET
379   observations. The mean annual cycle in NEE is not necessarily phased on that of GPP and RECO, the two latter
380   reaching their highest values from May to August in most sites. Significant differences are found between northern
381   (SE-Nor, FI-Let, FI-Hyy and SE-Svd) and southern (FR-FBn, IT-SR2 and FR-Bil) Europe, where ENF sites only
382   are available. The annual cycle is more marked and the sequestration period (i.e., month associated with negative
383   NEE values) is shorter in the former than the latter region. Temperature conditions (and light availability) are the
384   main drivers explaining these differences. In central Europe, where both ENF and DBF sites are available, there
385   is a clear impact of land cover class. The DBF sites show pronounced annual cycle with strong CO_2 uptake (below
386   -3 $tCO_2.ha^{-1}$) from May to August, and up to some extent in September, and strong CO_2 release the remaining
387   months (above 2 $tCO_2.ha^{-1}$). Conversely, the ENF sites show smoothed annual cycle: the summer peak of CO_2
388   sequestration barely exceeds -3 $tCO_2.ha^{-1}$ and the winter peak of CO_2 release rarely exceeds 1 $tCO_2.ha^{-1}$. Two sites
389   deviate from the general pattern: the DE-Hzd DBF site, which acts as a CO_2 source nearly year-round, and the DE-
390   RuW ENF site, which remains a consistent CO_2 sink on average.

391

392   The interannual variability of NEE, GPP, and RECO, as defined by the standard deviation metric, tends to be
393   stronger during the growing season (spring to fall) than in winter at almost all sites (Fig. 4b). The exact pattern
394   depends on the CO_2 flux, site and land cover class considered. GPP is always close to zero during winter in DBF
395   sites since trees are not photosynthetically active. This is not the case for ENF sites, particularly those located in
396   central Europe (DE-RuW and CZ-BK1). The interannual variability of RECO is substantial in summer only in
397   northern Europe. However, it can be non-negligible in other seasons in central and southern Europe. There,
398   significant differences between geographically close sites (e.g., FR-Bil and IT-SR2) suggest additional drivers
399   such as soil properties. The interannual variability of NEE is (i) weaker than that of GPP and RECO, likely due to
400   the strong coupling between GPP and RECO, (ii) primarily driven by RECO in winter and (iii) a complex response
401   of GPP and RECO in the remaining seasons. Note that the pattern of CO_2 flux interannual variability depends on
402   the metric used to assess it. When defined using the coefficient of variation, interannual variability is low in
403   summer and high in winter for GPP and RECO, with increasing variability toward the north. For NEE, variability
404   remains significant throughout the year, particularly from fall to winter (Fig. A1).
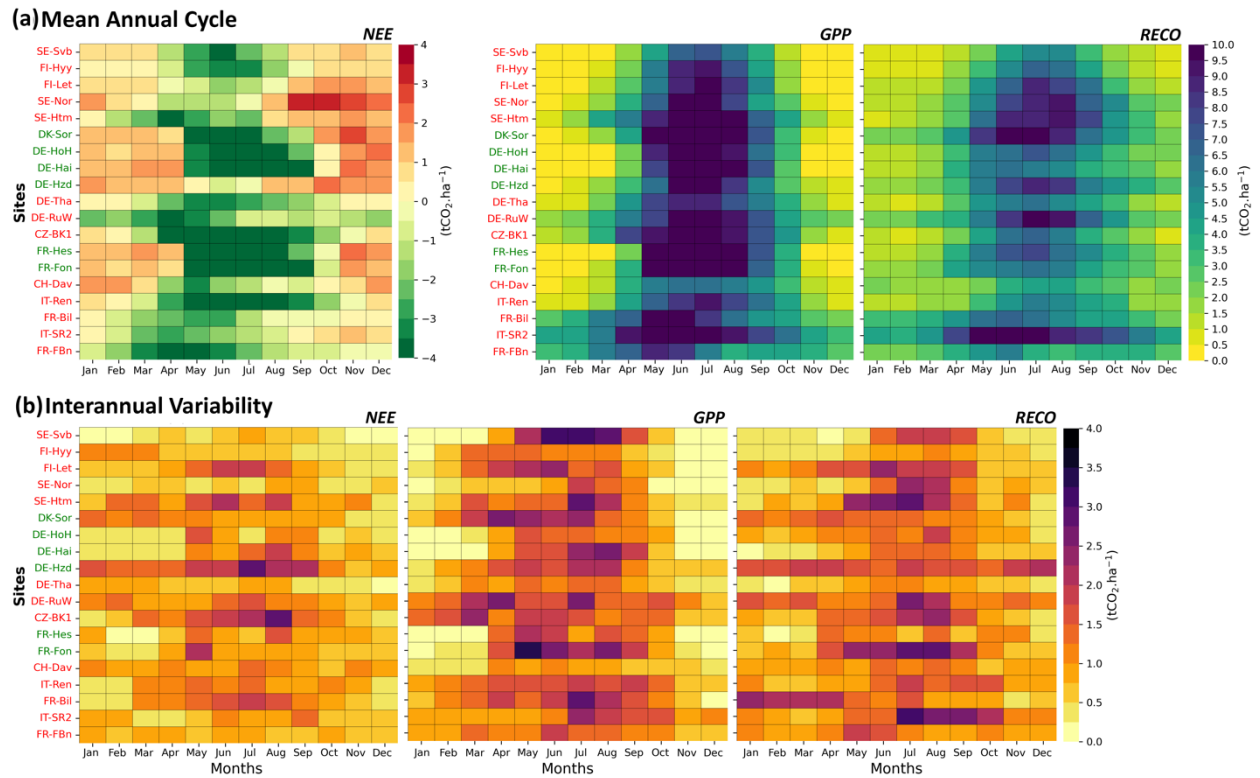
Figure 4. (a) Mean annual cycle and **(b)** interannual variability in monthly NEE, GPP and RECO (from left to right, respectively) as measured by eddy-covariance over the most extended available period for each site (see Table 1 for details). ENF sites are displayed in red text, while DBF sites are highlighted in green. Sites are ordered from north to south based on their latitude.

Overall, the mean annual cycle of observed CO_2 fluxes in European forests follows a clear spatial pattern driven by climate conditions and land cover class. In contrast, the interannual variability of observed CO_2 fluxes exhibits greater spatial noise across Europe and depends on the metric used. Nevertheless, it remains significant, highlighting the importance of assessing the impact of climate on it throughout the annual cycle.

3.2 Model evaluation in capturing the mean annual cycle and interannual variability of CO_2 fluxes

3.2.1 Mean annual cycle

The model skill in capturing the observed annual cycle and the magnitude in CO_2 fluxes is assessed in terms of correlation and mean bias, respectively (see section 2.3 for details). All models accurately capture the observed annual cycle of GPP and RECO, with correlation values often above 0.8 (Fig. 5a). The model skill is poorer but still correct for NEE, with correlation values remaining above 0.6 for most sites and models. The weaker correlation found for NEE compared to GPP and RECO is not surprising, as accurately estimating the NEE annual cycle requires precise estimation of both the temporal phasing and magnitude of GPP and RECO.
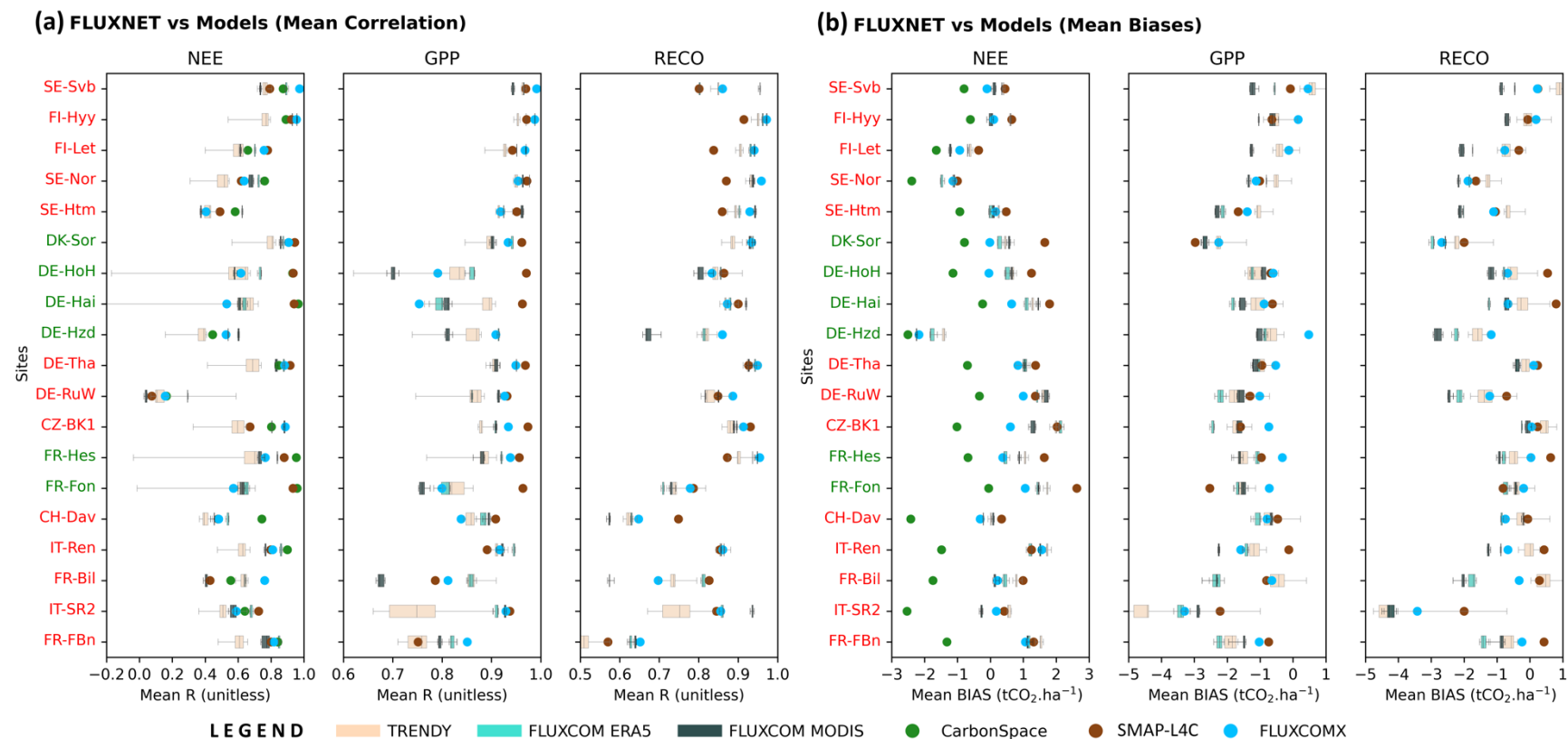
Figure 5. Model skill in capturing **(a)** the annual cycle and **(b)** magnitude of observed NEE, GPP and RECO. The model skill in capturing the annual cycle is assessed through the Bravais-Pearson correlation coefficient (R) calculated between the simulated and observed annual cycle of monthly CO_2 fluxes (12 values) for each year of the overlapping period. The multi-year mean R values are shown. The magnitude error is computed as the difference between simulated and observed CO_2 fluxes (model minus observation) for each month of the overlapping period. The mean magnitude error is shown. Results are displayed using colored dots for single member models (Carbon Space, FLUXCOM-X and SMAP-L4C) and boxplots for multi-member FLUXCOM models and the multi-model TRENDY ensemble. The boxes have lines at the lower quartile, median, and upper quartile values. The whiskers are lines extending from each end of the boxes to show the extent of the full range of the data, including outliers. The colour attributed to each model is detailed in the legend. ENF sites are displayed in red text, while DBF sites are highlighted in green. Sites are ordered from north to south based on their latitude.

436 Despite reasonable annual cycles, the models struggle in capturing the observed magnitude of RECO and GPP
437 (Fig. 5b). Three groups emerge. The first group includes the FLUXCOM (ERA5, MODIS and X) and TRENDY
438 models, which underestimate both GPP and RECO by about similar amounts, resulting in relatively "weak"
439 positive biases in NEE. The second group corresponds to the SMAP-L4C model, which overestimates RECO by
440 1 tCO_2 ha^{-1} $month^{-1}$ while underestimating GPP by the same amount, leading to a systematic underestimation of
441 CO_2 sequestration by approximately 2 tCO_2 ha^{-1} $month^{-1}$. The last group is the Carbon Space data-driven model,
442 which is the only model that systematically overestimates CO_2 sequestration, by up to 2.5 tCO_2 ha^{-1} $month^{-1}$.
443 However, the cause of this overestimation is unclear, as this model does not provide separate GPP and RECO
444 estimates.

446 Figure 5 highlights key insights into model behaviour. First, the data-driven and SMAP-L4C models generally
447 outperform the TRENDY models in capturing the annual cycle of CO_2 fluxes but do not necessarily provide better
448 estimates of flux magnitude. Second, models that accurately represent the annual cycle can still struggle with
449 magnitude. This is exemplified by the Carbon Space data-driven model, which ranks among the best for annual
450 cycle representation but severely overestimates CO_2 sequestration in many sites. Third, the machine learning
451 methods used in the FLUXCOM-ERA and FLUXCOM-MODIS ensembles have little impact on both the annual
452 cycle and magnitude of CO_2 fluxes. The input data itself appears to be more important, with the FLUXCOM
453 models accounting for both vegetation and climate (i.e., ERA5 and X) yielding more reliable results than those
454 accounting for vegetation alone (MODIS). Additionally, FLUXCOM-X improves upon the previous model
455 generation for most sites. Finally, the inter-model spread within the TRENDY ensemble is much smaller for CO_2
456 flux magnitude than for temporal variability, suggesting that the primary source of uncertainty in DGVMs lies in
457 the temporal phasing of the fluxes rather than their magnitude.

460 **3.2.2 Interannual variability**

462 We qualitatively evaluate how well the models capture the observed interannual variability of CO_2 fluxes in terms
463 of magnitude (monthly bias analysis) and temporal phasing (correlation analysis) over the overlapping period of
464 each model-observation pair.

466 All models strongly underestimate the magnitude in NEE interannual variability all year long (Fig. 6), particularly
467 during summer where biases often exceed 2.5 tCO_2 ha^{-1} $month^{-1}$. This is a well-known bias of current data-driven
468 and process-based models (e.g., Lin et al., 2023; Nelson et al., 2024). The only exception is the CarbonSpace
469 model that produce weak positive or negative biases at most sites.
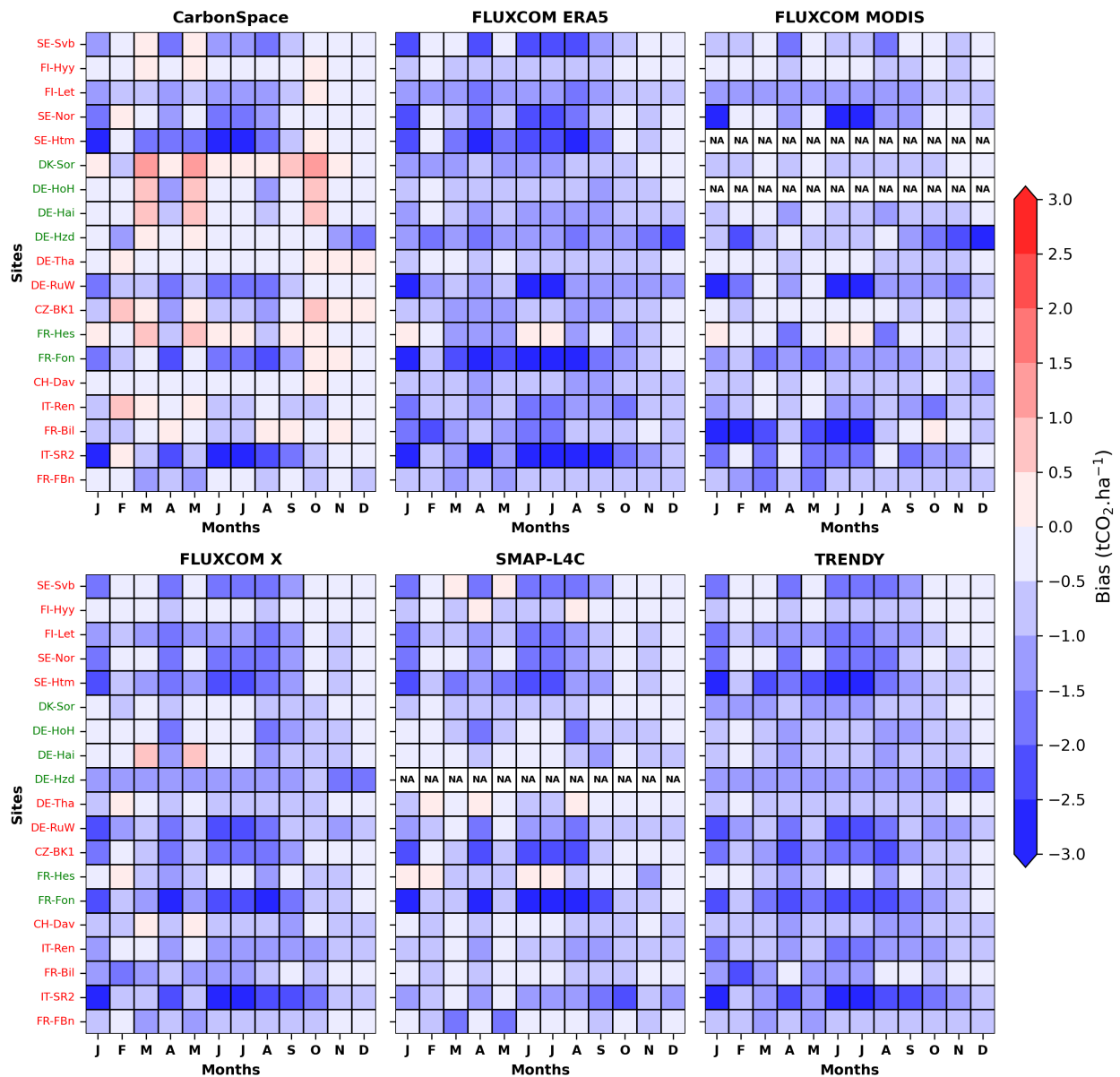
Figure 6. Model skill in capturing the observed magnitude in monthly NEE interannual variability. Model skill is assessed by computing biases between modelled and observed NEE interannual variability, as defined by the standard deviation of monthly fluxes. The number of years included varies depending on the model–observation pair, as shown in Fig. 2a. Cells labelled "NA" indicate cases where the overlap criterion is not met. For conciseness, biases are computed using the ensemble mean for FLUXCOM-ERA5, FLUXCOM-MODIS, and TRENDY models. ENF sites are displayed in red text, while DBF sites are highlighted in green. Sites are ordered from north to south based on their latitude.

Figure 7 shows the correlations between the modelled and observed interannual variability in monthly NEE. Correlation values are predominantly positive across Europe, though they are often low and not statistically significant (p > 0.05). The correlation values tend to be higher in fall for northern Europe sites and all year long in central Europe regardless of the model. The frequent lack of statistical significance in correlations can largely be attributed to the limited number of overlapping years. This is further supported by the fact that, except for Davos, correlation values tend to be higher and more likely to reach the 95% confidence level in model-observation pairs with a greater number of overlapping years (e.g., DK-Sor, DE-Hai and DE-Tha). Another challenge in capturing the observed temporal phasing of NEE interannual variability is that it requires accurately simulating the

interannual variability of both GPP and RECO. The latter is generally better represented by models than NEE variability itself (compare Fig. 7 with Figs. A2–A3). Scale inconsistencies may also contribute to the discrepancies. While flux tower observations reflect local variability, most models represent regional-scale fluxes (and drivers). This is supported by the Carbon Space model, the only site-scale model used in this study, which produces more satisfactory results, with positive correlation values for almost all sites and all months.
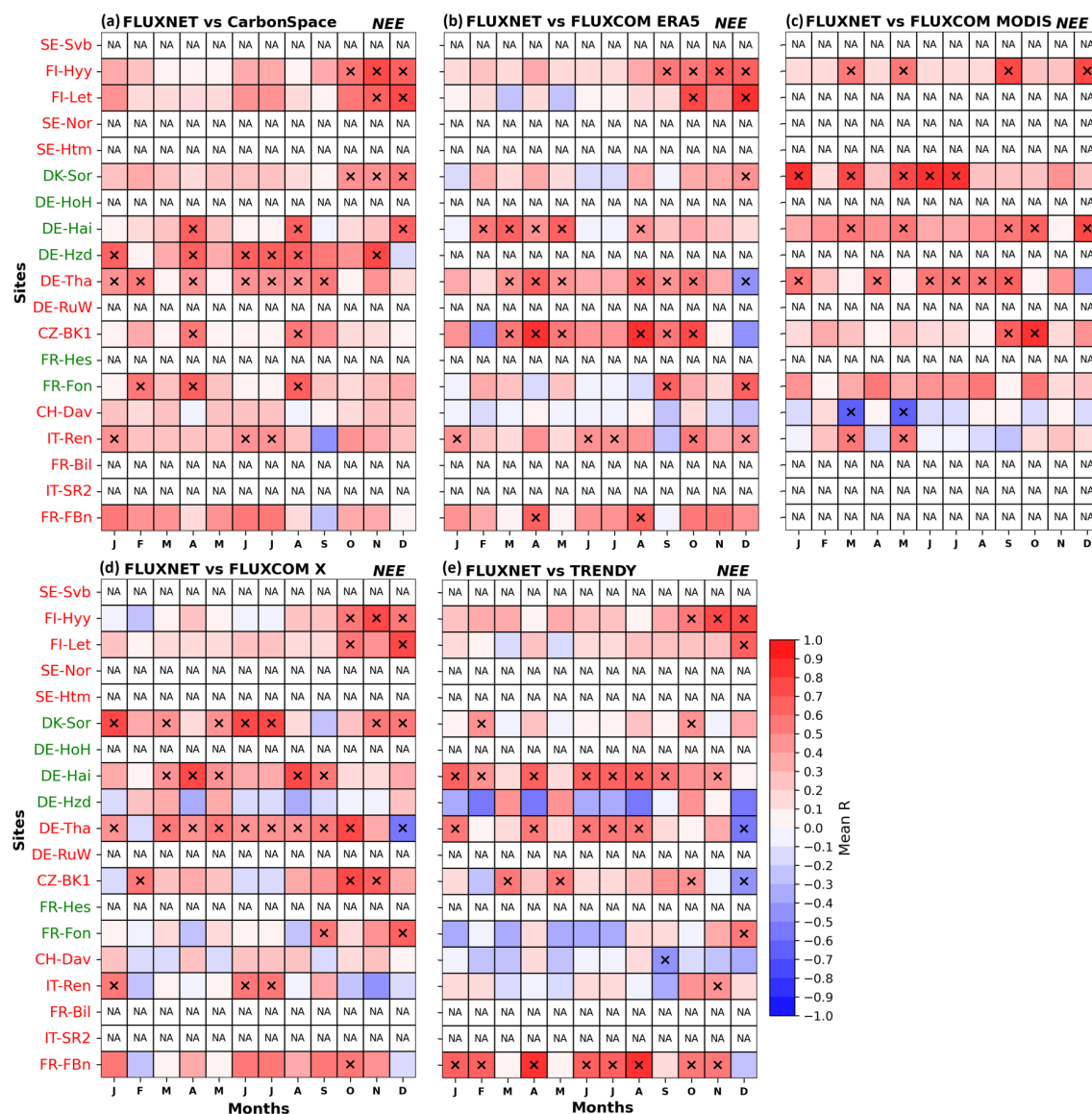
Figure 7. Model skill in capturing the observed temporal phasing in monthly NEE interannual variability. Model skill is assessed using the Bravais-Pearson correlation coefficient (R), calculated for each month where at least 10 years of overlap exists between each model–observation pair. The number of years included varies depending on the model–observation pair, as shown in Fig. 2a. Correlation values marked with "×" are significant at the 95% confidence level according to the Bravais-Pearson test. Cells labelled "NA" indicate cases where the overlap criterion is not met. For conciseness, the correlation analysis is performed using the ensemble mean for FLUXCOM-ERA5, FLUXCOM-MODIS, and TRENDY models. ENF sites are displayed in red text, while DBF sites are highlighted in green. Sites are ordered from north to south based on their latitude.

The spread among members of the FLUXCOM ensembles is low (not shown), regardless of whether they account for climate alone or both climate and vegetation. However, Figure 7 reveals significant differences between the

FLUXCOM products (ERA5, MODIS, and X; Fig. 7b–d). These differences are not necessarily due to the type of data used in these data-driven models, as the analysis periods differ between them. In contrast, the correlations between observations and the TRENDY ensemble mean (Fig. 7e) mask substantial variability among individual TRENDY models, with no single model consistently outperforming the others (Fig. A4).

These qualitative results suggest that the interannual variability of simulated NEE is at least partially aligned with that of observed CO_2 fluxes, supporting the use of models to assess the impact of climate on CO_2 flux interannual variability.

3.3 Climate – CO_2 flux relationship

3.3.1 Annual cycle

Figure 8 assesses the co-variability between the annual cycle of CO_2 fluxes and climate variables (T_{2m}, SM_{AVG}, and VPD) through correlation analysis. For conciseness, correlations are computed using the ensemble mean of CO_2 fluxes for FLUXCOM (ERA5 and MODIS) and TRENDY models. The inter-member dispersion in FLUXCOM and inter-model dispersion in TRENDY, shown in Fig. A5, are similar to those in Fig. 5 and are therefore not discussed here.

The annual cycle of CO_2 fluxes is closely linked to climate in both observations and models, as evidenced by statistically significant correlations at the 95% confidence level. The influence of climate on the annual cycle of CO_2 fluxes is generally stronger for GPP and RECO than for NEE, particularly for T_{2m} (Fig. 8a). Over Europe, GPP, RECO and CO_2 sequestration (i.e., negative NEE) tend to be higher when T_{2m} and VPD are high and SM_{AVG} is low. In turn, CO_2 fluxes are amplified in summer and damped in winter. Among the climate variables, T_{2m} and VPD exhibit stronger correlations with the CO_2 flux annual cycle than SM_{AVG}, reflecting their more pronounced seasonality (Fig. 3).

This climate – CO_2 flux relationship is particularly evident in northern and central Europe, where there is strong agreement between observations and models, as well as across different models. The only exception in central Europe is the Alpine site (CH-Dav), where SM_{AVG} is positively correlated with GPP and RECO and negatively correlated with NEE. This discrepancy arises because CH-Dav is the only site in the study where SM_{AVG} is higher in summer than in winter (Fig. 3b). In contrast, in southern Europe, the relationship between climate and NEE does not reach the 95% confidence level in observations. However, the models show a similar relationship to that found in northern and central Europe, albeit with weaker correlations. Whether this disagreement stems from the limited number of observational years available for these sites (7 to 13 years, see Table 1) or from an overestimation of climate impact on the CO_2 flux annual cycle remains an open question.
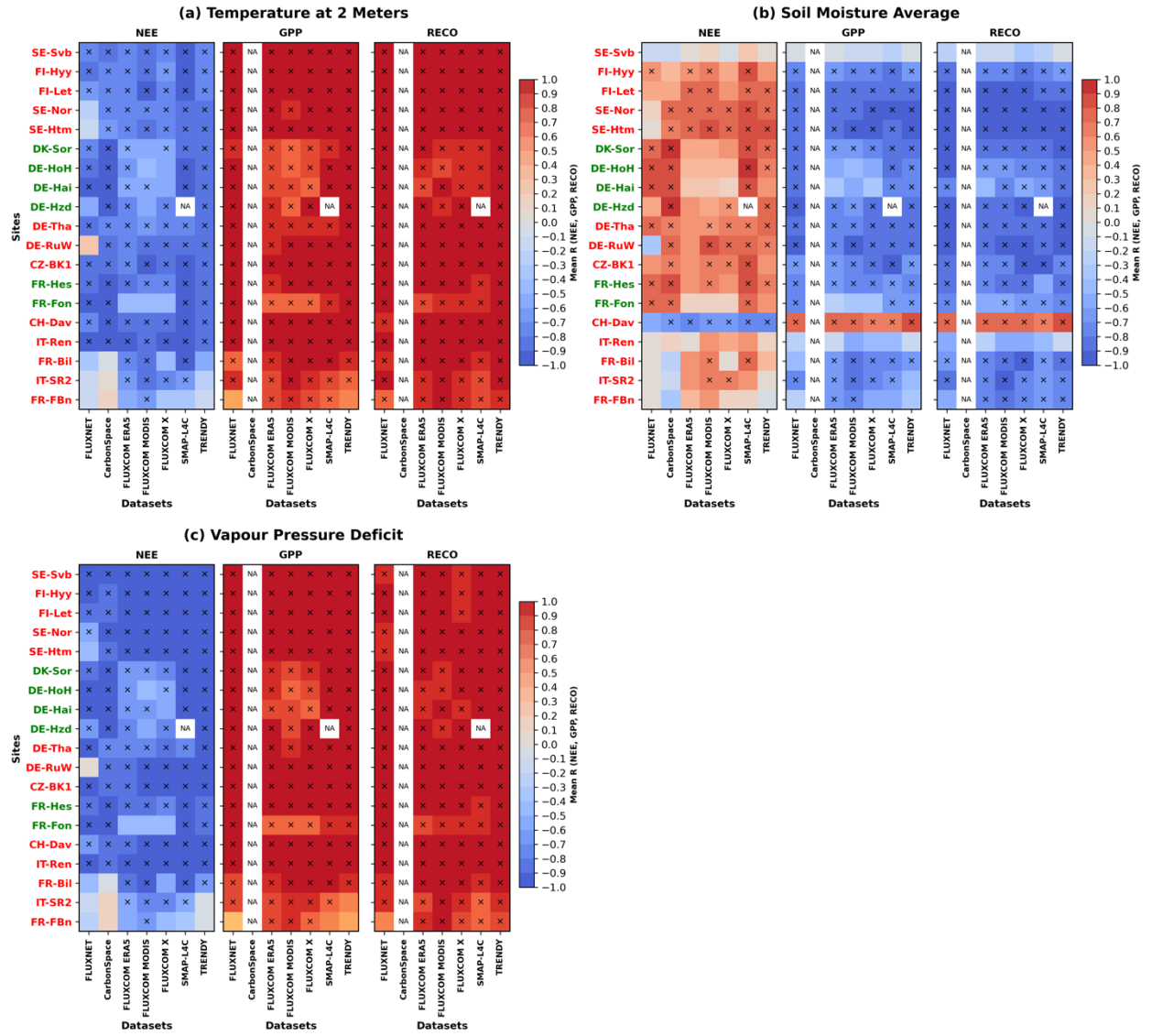
Figure 8. Co-variability in the annual cycle of CO_2 fluxes and **(a)** 2 m temperature, **(b)** soil moisture, and **(c)** vapour pressure deficit across all sites and datasets. Co-variability is assessed through Bravais-Pearson correlation, computed annually between CO_2 fluxes and ERA5-Land climate data, then averaged across years. The number of years included varies depending on the data, as shown in Fig. 2d. Correlation values marked with '×' are significant at the 95% confidence level according to the Bravais-Pearson test. Cells labelled 'NA' indicate cases where GPP and RECO are unavailable (CarbonSpace) or where CO_2 flux data are corrupted (SMAP-L4C). For conciseness, correlations are computed using the ensemble mean of CO_2 fluxes for FLUXCOM (ERA5 and MODIS) and TRENDY models. ENF sites are displayed in red text, while DBF sites are highlighted in green. Sites are ordered from north to south based on their latitude.

Figure 8 also reveals differences in model behaviour. First, the climate – CO_2 flux relationship appears sensitive to land cover class only in data-driven models. In the FLUXCOM models (ERA5, MODIS, X), this relationship is weaker for DBFs than ENFs in central Europe, whereas the Carbon Space model shows the opposite pattern. This sensitivity to land cover class may reflect model discrepancies, as the observed climate – CO_2 flux relationship does not depict such an ENF–DBF distinction. The reason for this discrepancy remains, however, unclear, given that these data-driven models are based on the same FLUXNET sites. Second, process-based models tend to overestimate the impact of climate on the annual cycle of CO_2 fluxes across all sites. For example, the SMAP-L4C model amplifies the influence of T_{2m} and SM_{AVG} on NEE, particularly in northern Europe (Fig. 8a-b). Meanwhile, in the TRENDY models, VPD emerges as the dominant driver of the NEE annual cycle (Fig. 8c). These results

567 suggest that process-based models may underestimate the role of additional factors, such as soil properties, in
568 shaping the CO_2 flux annual cycle.
569
570

571 **3.3.2 Interannual variability**

572
573 We now investigate the interannual co-variability between CO_2 fluxes and climate, with a particular focus on how
574 this relationship evolves throughout the annual cycle. Figure 9 illustrates the interannual relationship between
575 climate and NEE for each month through correlation analysis. The relationship is notably noisier in the
576 observations compared to the models, due to the limited observational record and site-specific variations in
577 measurement periods, and highlights model sensitivity. Nonetheless, the general pattern remains consistent,
578 showing distinct differences between northern/central Europe and southern Europe.

579
580 In northern and central Europe, the correlation patterns of NEE with T_{2m} and VPD are similar (Fig. 9a and c),
581 highlighting the strong coupling between these two climate variables. The NEE interannual variability is correlated
582 positively with T_{2m}, VPD and, to a lesser extent, SM_{AVG} in winter and fall. This means that anomalously high T_{2m},
583 VPD and SM_{AVG} favor CO_2 release during the cold seasons. This pattern is similar for GPP and RECO (Figs. A6-
584 A7), but correlations are stronger for RECO, highlighting its significant contribution to NEE interannual variability
585 during the cold seasons. In spring (March–May), the relationship between NEE and T_{2m}/VPD reverses compared
586 to the cold season pattern, meaning that anomalously low T_{2m} and VPD promote CO_2 sequestration. The NEE–
587 SM_{AVG} relationship, however, varies between northern and central Europe. In northern Europe, depending on the
588 dataset, SM_{AVG} and NEE interannual variability are not consistently linked, with correlations either weak and
589 insignificant or strong but inconsistent throughout the spring season (Fig. 9b). In contrast, a clear relationship
590 emerges in central Europe, where correlations are significantly positive across most sites and datasets, though their
591 strength remains uncertain (with SMAP-L4C showing much larger correlation values). The increase in spring CO_2
592 sequestration under anomalously dry soil conditions is likely driven by elevated T_{2m} and VPD, leading to enhanced
593 evapotranspiration and drier soils. During the peak of the summer season (July–August), NEE is positively
594 correlated with T_{2m} and VPD and negatively correlated with soil moisture across most sites in northern and central
595 Europe.
596
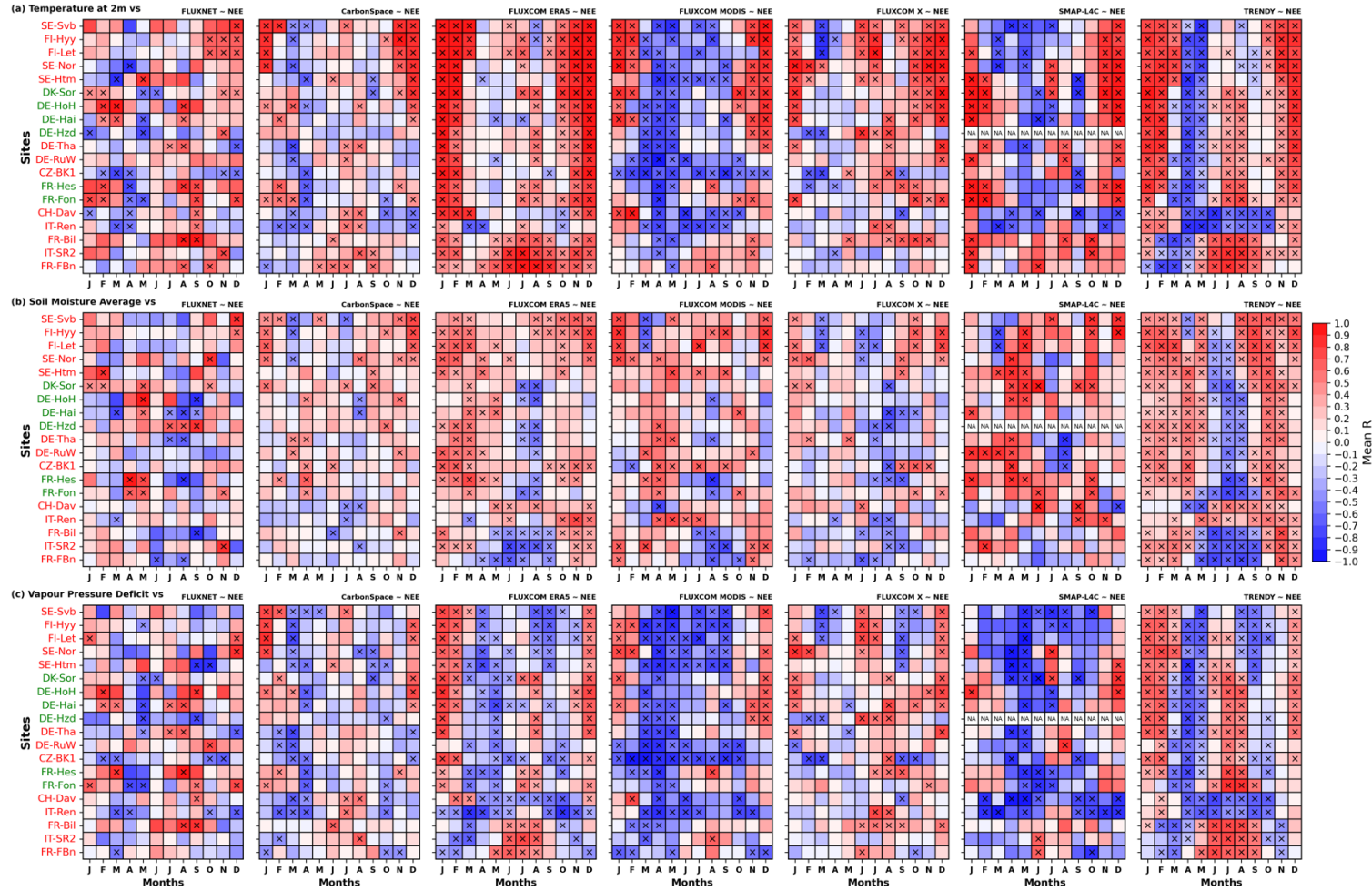
Figure 9. Interannual co-variability between NEE and **(a)** 2 m temperature, **(b)** soil moisture and **(c)** vapour pressure deficit for each month, all sites and all datasets. The co-variability is assessed through Bravais Pearson correlation computed for each month between CO_2 fluxes and ERA5-Land climate data. The number of years included varies depending on the data, as shown in Fig. 2d. Correlation values marked with '×' are significant at the 95% confidence level according to the Bravais-Pearson test. Cells labelled 'NA' indicate cases where CO_2 flux data are corrupted (SMAP-L4C). For conciseness, correlations are computed using the ensemble mean of CO_2 fluxes for FLUXCOM (ERA5 and MODIS) and TRENDY models. ENF sites are displayed in red text, while DBF sites are highlighted in green. Sites are ordered from north to south based on their latitude.

603 In southern Europe (FR-Bil, IT-SR2, and FR-FBn), the influence of climate on NEE interannual variability is more
604 uncertain, particularly for T_{2m} and VPD, as both the sign and strength of their correlations with NEE vary across
605 datasets. Correlations are generally weak and/or barely significant in the observations, the CarbonSpace model,
606 FLUXCOM-MODIS, and SMAP-L4C models. In FLUXCOM-ERA5, the correlation signs for T_{2m} and VPD are
607 inconsistent (except in summer), whereas in TRENDY, they remain consistent except in fall. This inconsistency
608 is not observed for GPP and RECO (Figs. A6–7). In summer, most datasets indicate that anomalously low T_{2m} and
609 VPD, along with anomalously high SM_{AVG}, enhance both GPP and RECO. This suggests that NEE interannual
610 variability in southern Europe results from a complex interplay between GPP and RECO contributions. Moreover,
611 the opposing correlation signs between NEE–T_{2m} and NEE–VPD in southern Europe suggest that VPD in drier,
612 hotter environments is more strongly influenced by atmosphere-surface feedbacks than by large-scale atmospheric
613 conditions. In contrast, the impact of SM_{AVG} on NEE interannual variability shows greater inter-dataset agreement
614 (Fig. 9b), with positive correlations in winter and fall and negative correlations in summer. This indicates that
615 excess winter precipitation, leading to wetter soils, enhances CO_2 release, whereas increased summer precipitation
616 or reduced evapotranspiration promotes CO_2 sequestration.

617
618

619 **4 Discussion**

620
621 This study aims at assessing the impact of climate on annual cycle and interannual variability of monthly CO_2
622 fluxes in European DBFs and ENFs through conjointly analysing observations from the FLUXNET network and
623 state-of-the-art data-driven and process-based models.

624
625 As a first step, we assess the model abilities to reproduce the observed mean annual cycle and interannual
626 variability of CO_2 fluxes. This evaluation presents two key challenges. First, the temporal coverage of observations
627 in the FLUXNET database is often limited, making it difficult to extract robust signals, particularly for interannual
628 variability. Second, there is a spatial scale mismatch between site-level observations, representing fluxes from the
629 tower footprint to several square kilometers (Göckede et al., 2008), and most models used in this study, which
630 simulate fluxes at regional to large scales, except for the hectometric-scale CarbonSpace model. Given these
631 constraints, our evaluation should be considered qualitative rather than strictly quantitative.

632
633 The models reasonably capture both the annual cycle and interannual variability of observed CO_2 fluxes, though
634 with some magnitude discrepancies. In particular, the models accurately capture the north-to-south gradient, with
635 increased length in the CO_2 sequestration period from northern to southern Europe, as well as the more pronounced
636 annual cycle in DBFs than ENFs. With the exception of the CarbonSpace model, which overestimates CO_2
637 sequestration across all European sites, most models tend to underestimate GPP and overestimate RECO, resulting
638 in a near systematic underestimation of CO_2 sequestration.

639
640 The interannual variability in the models is weaker than in the observations, consistent with previous studies (e.g.,
641 Nelson et al., 2024). Yet, the co-variability between observed and simulated CO_2 fluxes remains correct despite
642 the aforementioned constraints. This agreement was expected for data-driven models, as they incorporate

643   FLUXNET observations in their development. However, it was less anticipated for process-based models, which

644   do not assimilate direct CO_2 flux measurements. Their ability to capture observed interannual variability likely

645   stems from the fact that TRENDY models are driven by observed CO_2 concentrations, land-use changes, and

646   climate data, while the SMAP-L4C model benefits from the assimilation of satellite-derived soil moisture

647   observations.

648

649   Despite uncertainties, our results highlight that state-of-the-art models are valuable tools for complementing

650   observations, particularly in assessing the impact of climate on the interannual variability of CO_2 fluxes by

651   significantly expanding the number of studied years and the spatial domain. The relationship between CO_2 fluxes

652   and climate is analysed for both the annual cycle and interannual variability using synchronous correlation analyses

653   between each CO_2 flux and individual climate variables, including 2 m temperature (T_{2m}), vapour pressure deficit

654   (VPD), and soil moisture (SM_{AVG}).

655

656   Regarding the annual cycle, the influence of climate on CO_2 fluxes is stronger in northern and central Europe than

657   in southern Europe, where seasonal climate variations are less pronounced. In southern Europe, both the agreement

658   between observations and models and the consistency among different data-driven and process-based models are

659   weaker. The spread within members (FLUXCOM-ERA5 and FLUXCOM-MODIS), and DVGMs (TRENDY), is

660   also larger. We hypothesize that part of this model uncertainty stems from the limited number of ENF sites in

661   southern Europe, leading to weak constraints for data-driven models and fewer reference points for calibrating

662   DVGMs. However, it is worth noting that the uncertainty associated with the machine learning methods used to

663   develop data-driven models remains low, whereas inter-DGVM spread can be substantial.

664

665   Regarding interannual variability, the climate impact on CO_2 fluxes can be summarized in three points. First,

666   climate impacts more strongly GPP and RECO than NEE, regardless of the site and dataset. Since NEE is the

667   difference between GPP and RECO, its interannual variability arises from various combinations of these two

668   components. For instance, reduced CO_2 sequestration can results from a greater increase in RECO compared to

669   GPP, a larger decrease in GPP than in RECO, a decrease in GPP with no change in RECO, or an increase in RECO

670   without any change in GPP. Such as complexity implies that the influence of climate on NEE is less direct and

671   likely more intricate than its effects on GPP and RECO. Second, the climate impact significantly changes along

672   the annual cycle with noticeable differences between northern/central and southern Europe, regardless of land

673   cover class. For conciseness, we discuss only results for NEE. In northern and central Europe, CO_2 sequestration

674   is closely linked to T_{2m} and VPD, whereas in southern Europe, soil moisture emerges as the dominant driver. These

675   findings reinforce the role of soil moisture as the primary control on NEE in southern Europe, though not

676   necessarily on its components (i.e., GPP and RECO), refining previous studies (Seddon et al., 2016; Madani et al.,

677   2017). In northern and central Europe, most models indicate that CO_2 sequestration is enhanced by anomalously

678   low T_{2m} and VPD and anomalously high SM_{AVG} in summer, whereas the opposite pattern prevails in spring. This

679   finding aligns with previous case studies showing that heatwaves and droughts reduce summer CO_2 sequestration

680   (Ciais et al., 2005; Smith et al., 2020; Thompson et al., 2020; van der Woude et al., 2023). It also highlights that

681   anomalously warm and dry springs may, in some cases, enhance CO_2 sequestration, likely because soil moisture

682   levels remain sufficient during this period, in line with e.g. Delpierre et al. (2009) and Smith et al. (2020). Such a

683 transition from spring to summer is less evident in southern Europe, which instead exhibits contrasting patterns
684 between late fall–winter and early spring–early fall.
685
686 Finally, we acknowledge that the general patterns discussed above do not always hold at specific sites. This
687 suggests the influence of additional factors, such as soil properties, forest management practices, tree age and tree
688 species (see references in the Introduction). Assessing the impact of these factors on CO_2 flux variability falls
689 beyond the scope of this study, as it would require detailed site-specific information not available in the FLUXNET
690 database and not fully represented in the models used.
691
692

693 **5 Conclusion**
694

695 This study makes use of state-of-the-art data-driven and process-based models to complement observations for
696 assessing the impact of climate on the annual cycle and interannual variability of monthly CO_2 fluxes in European
697 DBFs and ENFs. Output from different data-driven models (CarbonSpace and FLUXCOM-ERA5, -MODIS and
698 -X) and process-based models forced by realistic conditions (assimilation of satellite derived soil moisture in
699 SMAP-L4C and time-varying CO_2 concentration, land-use and climate in TRENDY DVGMs) are analysed
700 conjointly with CO_2 measurements from 19 sites (6 DBFs and 13 ENFs) of the FLUXNET network. Across
701 Europe, a clear north-south gradient emerges in the annual cycle of CO_2 fluxes. The length of the CO_2 sequestration
702 season increases southwards in link with more favourable climate conditions for photosynthesis in southern than
703 northern Europe. This large-scale pattern is perturbed locally by site elevation and other site factors not included
704 in the study (e.g., soil properties and forest age). It is also perturbed by land cover class, with more pronounced
705 annual cycle of DBFs than ENFs in central Europe. The interannual variability of CO_2 fluxes does not exhibit such
706 a north-south gradient, regardless of the metric used (standard deviation or coefficient of variation). However, it
707 remains strong across all seasons, with spring and summer showing high variability based on standard deviation,
708 and autumn and winter based on the coefficient of variation.
709

710 The models accurately capture the observed features despite magnitude differences. Compared to observations,
711 the CO_2 sequestration is weaker in regional-scale models and stronger in the hectometric-scale CarbonSpace data-
712 driven model. All models underestimate the interannual variability of CO_2 fluxes, as already reported (Lin et al.
713 2023; Nelson et al., 2024). However, the interannual variability of modelled fluxes correlates well with the
714 observations. This supports the use of models to complement observations, whose limited temporal coverage
715 hinders the assessment of climate impacts on CO_2 interannual variability. The influence of climate on CO_2 flux
716 interannual variability changes along the annual cycle and a clear distinction emerges between northern/central
717 Europe and southern Europe despite model dependencies. Atmospheric factors (i.e., 2 m temperature and vapour
718 pressure deficit) dominate CO_2 fluxes interannual variability in northern and central Europe, while soil moisture
719 dominates in southern Europe. Winter and fall CO_2 release increases under elevated temperature and VPD in
720 northern and central Europe and under low VPD in southern Europe. The CO_2 sequestration increases under
721 anomalously hot and dry conditions in spring and cold and wet conditions in summer in northern/central Europe.
722 Anomalously cold and wet conditions also favor CO_2 sequestration in southern Europe from May to September.

723

724   These results highlight the significant space-time variability in the impact of climate on forest CO_2 fluxes across

725   Europe. This variability underscores the importance of considering regional and seasonal differences when

726   assessing the effects of climate change on CO_2 fluxes. Neglecting these variations could lead to oversimplified

727   conclusions and hinder the development of accurate predictions and effective mitigation strategies.

728

729 **Appendices**

730

731

732 **Table A1.** List of TRENDY DVGMs used in this study.

DVGM	Reference
CABLE-POP	Haverd et al. (2018)
CLM5.0	Lawrence et al. (2019)
DLEM	Tian et al. (2016)
JULES	Best et al. (2011); Clark et al. (2011)
LPX-Bern	Lienert and Joos (2018)
OCN	Zaehle et al. (2010)
ORCHIDEE	Krinner et al. (2005)
SDGVM	Woodward and Lomas (2004)
ISBA-CTRIP	Delire et al. (2020)
IBIS	Xia et al. (2015); Jinxun et al. (2022)
CLASSIC	Seiler et al. (2021)
EDv3	Longo et al. (2019)
E3SM	Golaz et al. (2019)
LPJmL	Bondeau et al. (2007)
LPJwsl	Gerten et al. (2004)

Columns 1 and 2 provide the name of the DGVM and its corresponding reference, respectively.

733
734
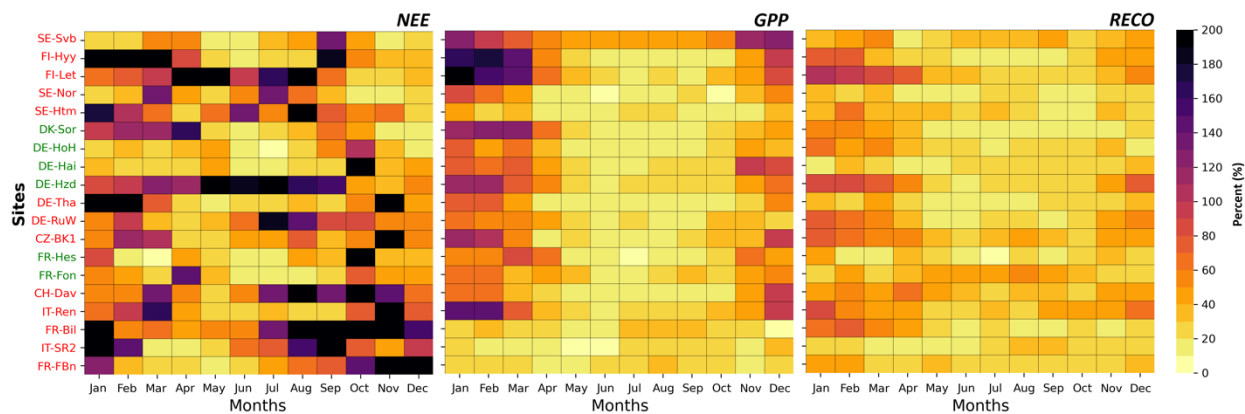
735
736 **Figure A1.** Same as Fig. 4b but using the coefficient of variation as a metric for interannual variability.
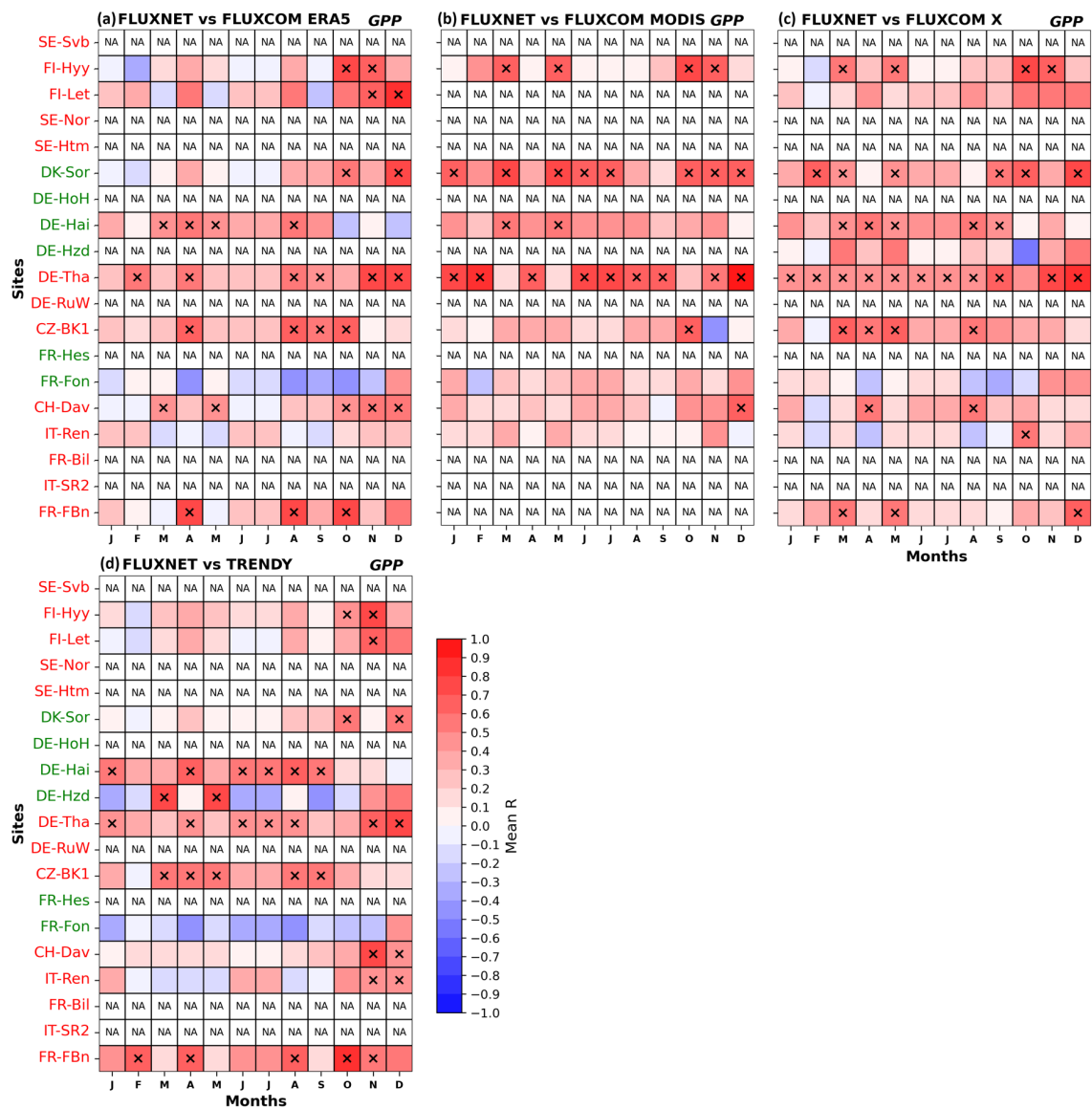
Figure A2. Same as Fig. 7 but for GPP.
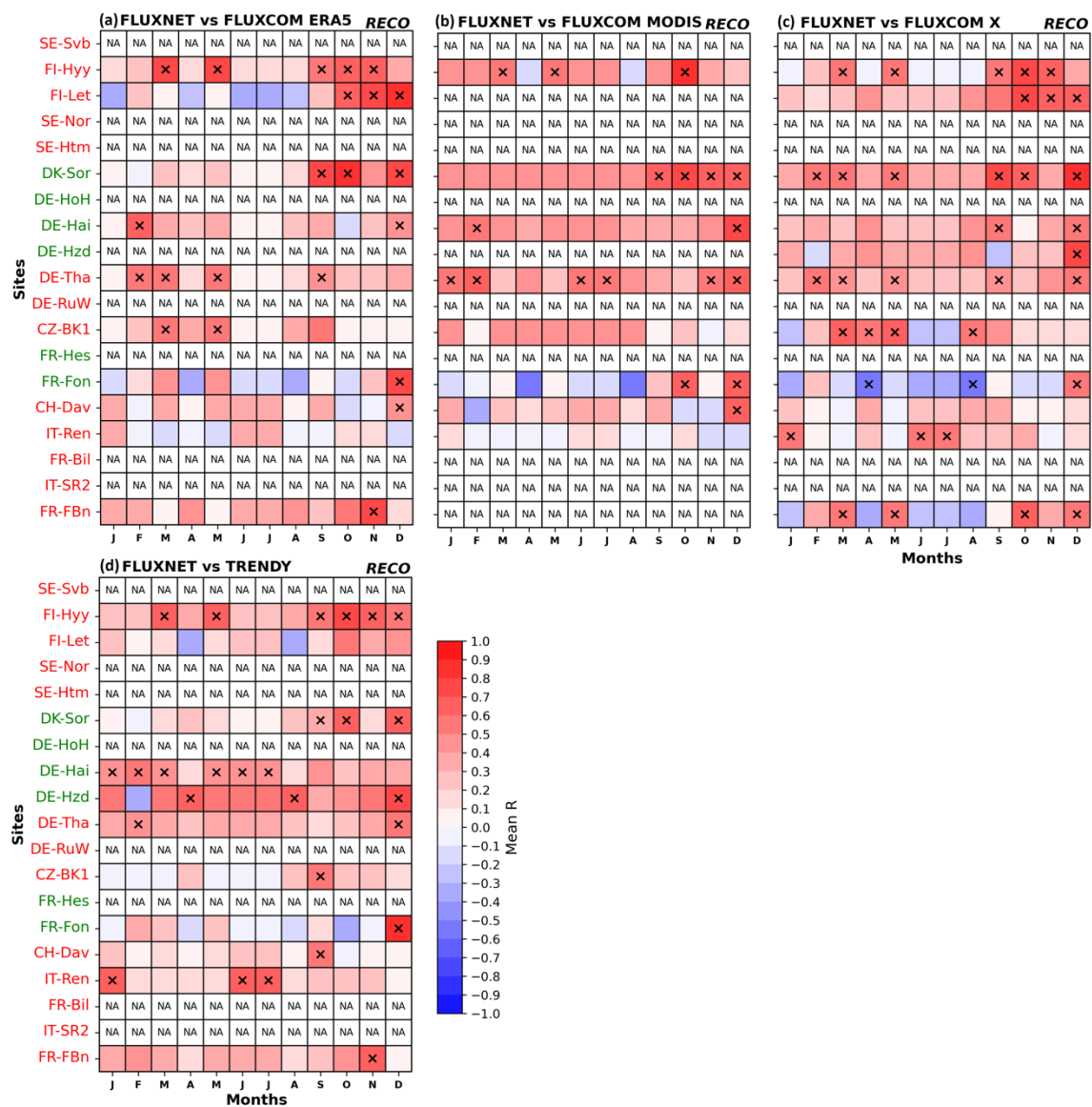
739
740 **Figure A3.** Same as Fig. 7 but for RECO.
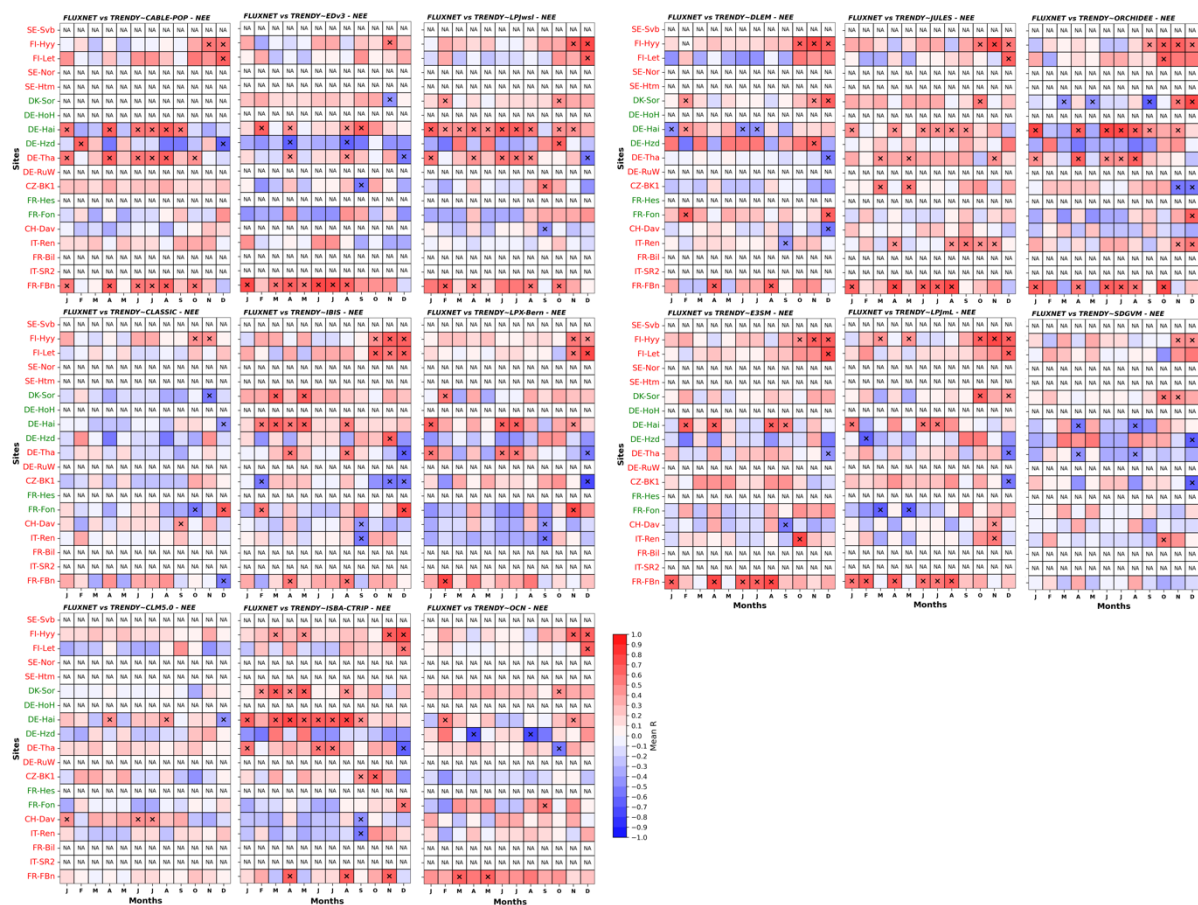
Figure A4. Same as Fig. 7e but for each TRENDY model considered in this study.

743
744 **Figure A5.** Same as Fig. 5 but for the relationship between the annual cycle of CO_2 fluxes and (a) 2 m temperature,
745 (b) soil moisture, and (c) vapour pressure deficit. This relationship is evaluated using Bravais-Pearson correlation.
746 For details, refer to the legend caption of Fig. 8.
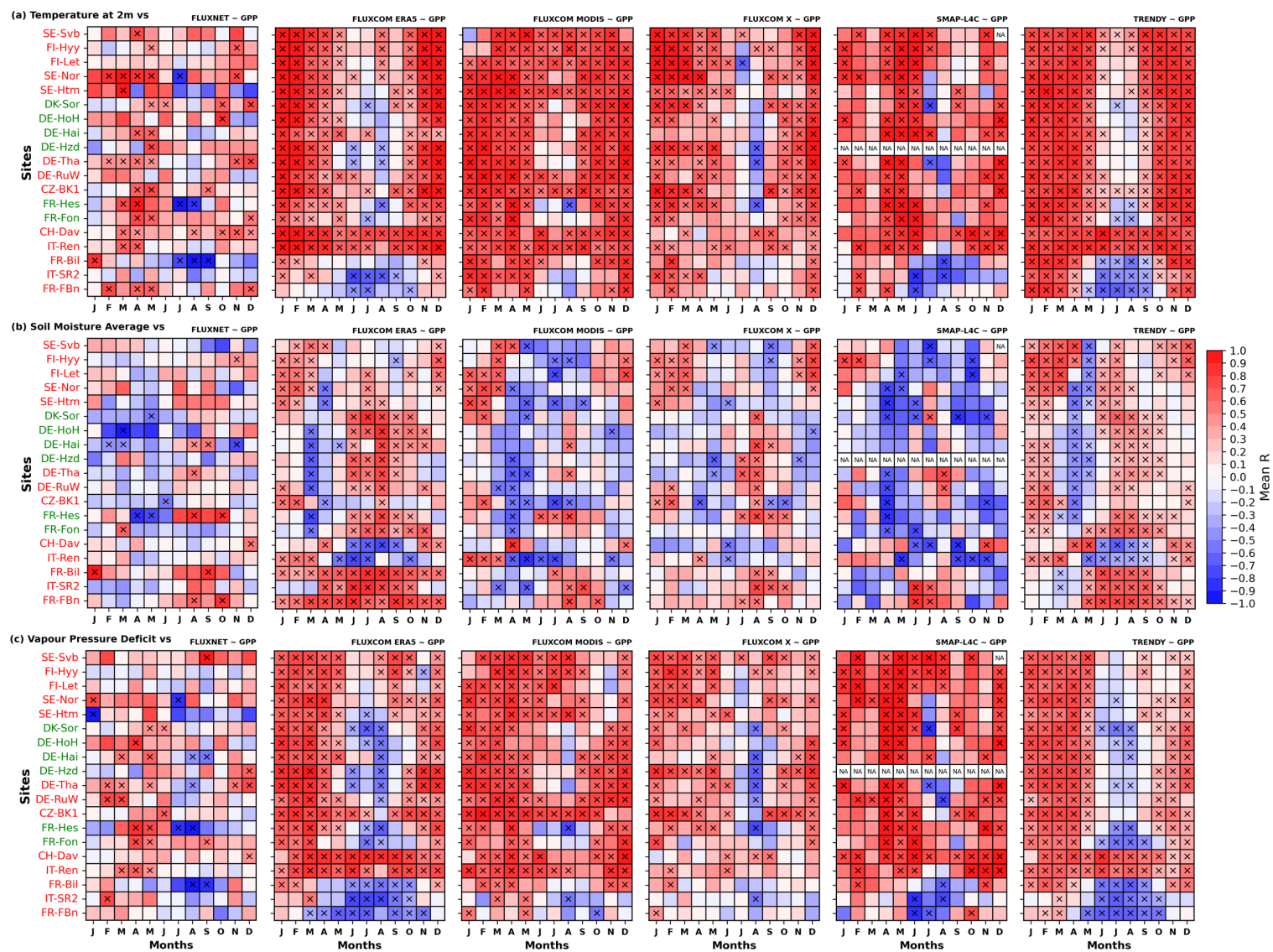
747
748   **Figure A6.** Same as Fig. 9 but for GPP.
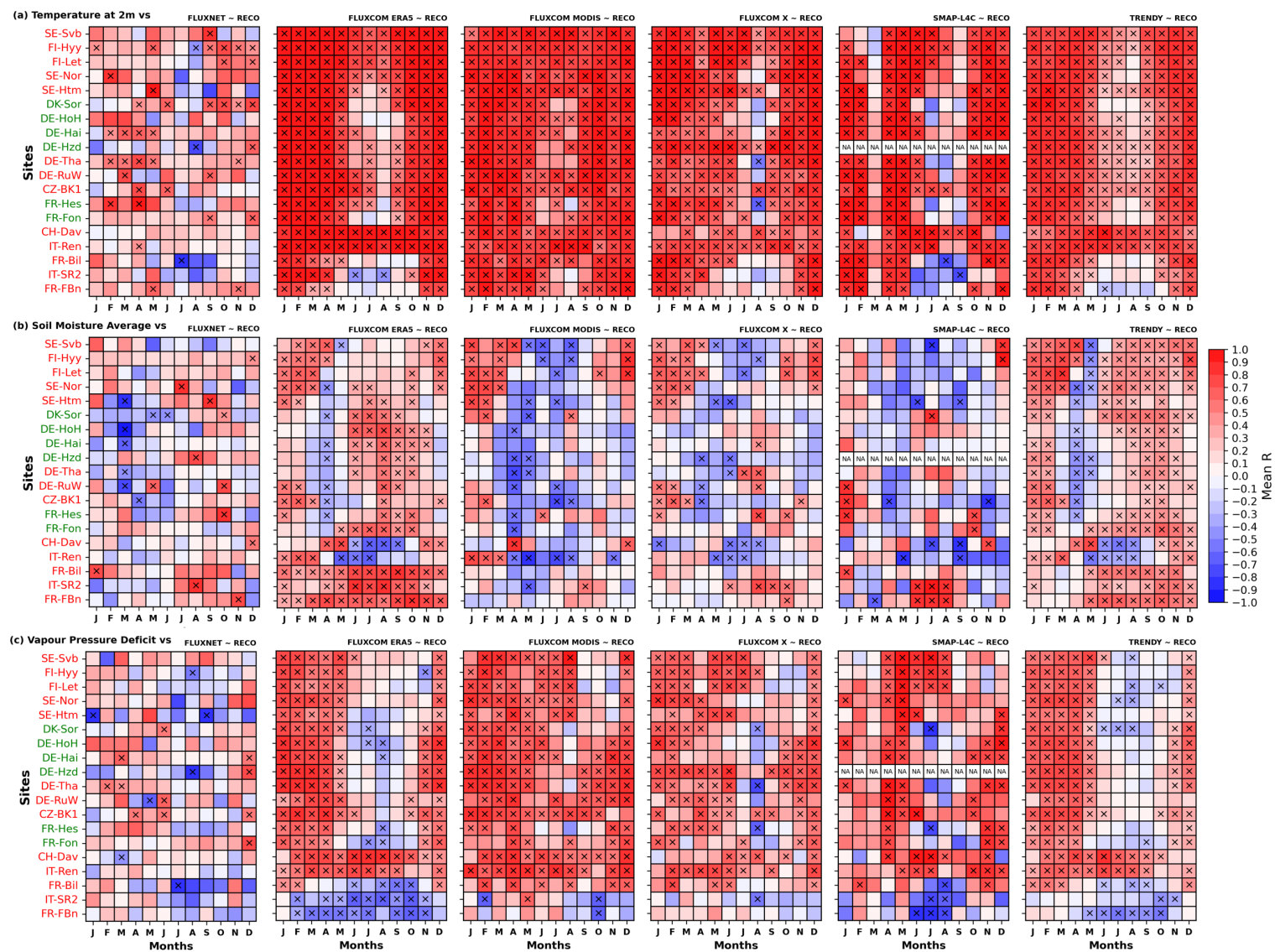
749
750   **Figure A7.** Same as Fig. 9 but for GPP.

Author contribution

JC conceived the study. JC, AU, and GM collected the data and developed the analysis scripts. GM and JC drafted the first version of the manuscript. AU and JC drafted the second version. All co-authors contributed to its review.

Acknowledgement

This work is funded by the French National Research Agency (ANR-22-CPJ2-0026-01) and is part of the "Laboratoire d'expérimentation forestière du mont Beuvray", supported by the European Union (EAFRD) and the Région Bourgogne-Franche-Comté, as part of the agricultural European Innovation Partnership (EIP-AGRI). We thank Daniel Berveiller for useful discussions on eddy covariance measurements and the two anonymous reviewers for constructive comments.

Data Availability

Climate parameters from the ERA5-Land are available at https://cds.climate.copernicus.eu/datasets/reanalysis-era5-land. CO_2 fluxes from the FLUXOM data-driven model are available at https://www.bgc-jena.mpg.de and https://meta.icos-cp.eu/collections/zfwf1Ak2I7OlziGDTX8Xl6_T. Those from TRENDY and SMAP-L4C process-based models are available on request to Professor Stephan Sitch (s.a.sitch@exeter.ac.uk) and at https://nsidc.org/data/spl4cmdl/versions/7, respectively.

Conflict of Interest

The authors declare no competing interests.

References

Besnard, S., Carvalhais, N., Arain, M. A., Black, A., De Bruin, S., Buchmann, N., Cescatti, A., Chen, J., Clevers, J. G. P. W., Desai, A. R., Gough, C. M., Havrankova, K., Herold, M., Hörtnagl, L., Jung, M., Knohl, A., Kruijt, B., Krupkova, L., Law, B. E., Lindroth, A., Noormets, A., Roupsard, O., Steinbrecher, R., Varlagin, A., Vincke, C., and Reichstein, M.: Quantifying the effect of forest age in annual net forest carbon balance,

786   Environ. Res. Lett., 13, https://doi.org/10.1088/1748-9326/AAEAEB, 2018.

787   Best, M. J., Pryor, M., Clark, D. B., Rooney, G. G., Essery, R. . L. H., Ménard, C. B., Edwards, J. M., Hendry, M.
788   A., Porson, A., Gedney, N., Mercado, L. M., Sitch, S., Blyth, E., Boucher, O., Cox, P. M., Grimmond, C. S.
789   B., and Harding, R. J.: The Joint UK Land Environment Simulator (JULES), model description – Part 1:
790   Energy and water fluxes, Geosci. Model Dev., 4, 677–699, https://doi.org/10.5194/GMD-4-677-2011, 2011.
791

792   Bondeau, A., Smith, P. C., Zaehle, S., Schaphoff, S., Lucht, W., Cramer, W., Gerten, D., Lotze-campen, H., Müller,
793   C., Reichstein, M., and Smith, B.: Modelling the role of agriculture for the 20th century global terrestrial
794   carbon balance, Glob. Chang. Biol., 13, 679–706, https://doi.org/10.1111/J.1365-2486.2006.01305.X, 2007.
795

796   Burba,   G.:   Atmospheric   flux   measurements,   Adv.   Spectrosc.   Monit.   Atmos.,   443–520,
797   https://doi.org/10.1016/B978-0-12-815014-6.00004-X, 2021.
798

799   Cai, W. and Prentice, I. C.: Recent trends in gross primary production and their drivers: analysis and modelling at
800   flux-site and global scales, Environ. Res. Lett., 15, 124050, https://doi.org/10.1088/1748-9326/ABC64E,
801   2020.
802

803   Carrara, A., Kowalski, A. S., Neirynck, J., Janssens, I. A., Yuste, J. C., and Ceulemans, R.: Net ecosystem CO_2
804   exchange of mixed forest in Belgium over 5 years, Agric. For. Meteorol., 119, 209–227,
805   https://doi.org/10.1016/S0168-1923(03)00120-5, 2003.
806

807   Carrara, A., Janssens, I. A., Curiel Yuste, J., and Ceulemans, R.: Seasonal changes in photosynthesis, respiration
808   and   NEE   of   a   mixed   temperate   forest,   Agric.   For.   Meteorol.,   126,   15–31,
809   https://doi.org/10.1016/J.AGRFORMET.2004.05.002, 2004.
810

811   Chen, T., and Guestrin C.: Xgboost: A scalable tree boosting system. In Proceedings of the 22nd ACM SIGKDD
812   international   conference   on   knowledge   discovery   and   data   mining,   785–794.
813   https://doi.org/10.1145/2939672.2939785, 2016.
814

815   Ciais, P., Reichstein, M., Viovy, N., Granier, A., Ogée, J., Allard, V., Aubinet, M., Buchmann, N., Bernhofer, C.,
816   Carrara, A., Chevallier, F., De Noblet, N., Friend, A. D., Friedlingstein, P., Grünwald, T., Heinesch, B.,
817   Keronen, P., Knohl, A., Krinner, G., Loustau, D., Manca, G., Matteucci, G., Miglietta, F., Ourcival, J. M.,
818   Papale, D., Pilegaard, K., Rambal, S., Seufert, G., Soussana, J. F., Sanz, M. J., Schulze, E. D., Vesala, T., and
819   Valentini, R.: Europe-wide reduction in primary productivity caused by the heat and drought in 2003, Nat.
820   2005 4377058, 437, 529–533, https://doi.org/10.1038/nature03972, 2005.
821

822   Clark, D. B., Mercado, L. M., Sitch, S., Jones, C. D., Gedney, N., Best, M. J., Pryor, M., Rooney, G. G., Essery,
823   R. L. H., Blyth, E., Boucher, O., Harding, R. J., Huntingford, C., and Cox, P. M.: The Joint UK Land
824   Environment Simulator (JULES), model description – Part 2: Carbon fluxes and vegetation dynamics, Geosci.
825   Model Dev., 4, 701–722, https://doi.org/10.5194/GMD-4-701-2011, 2011.
826

827   Curtis, P. S. and Gough, C. M.: Forest aging, disturbance and the carbon cycle, New Phytol., 219, 1188–1193,
828   https://doi.org/10.1111/NPH.15227, 2018.
829

830   Delire, C., Séférian, R., Decharme, B., Alkama, R., Calvet, J. C., Carrer, D., Gibelin, A. L., Joetzjer, E., Morel,
831   X., Rocher, M., and Tzanos, D.: The Global Land Carbon Cycle Simulated With ISBA-CTRIP: Improvements
832   Over   the   Last   Decade,   J.   Adv.   Model.   Earth   Syst.,   12,   e2019MS001886,
833   https://doi.org/10.1029/2019MS001886, 2020.
834

835   Delpierre, N., Soudani, K., François, C., Köstner, B., Pontailler, J. Y., Nikinmaa, E., Misson, L., Aubinet, M.,
836   Bernhofer, C., Granier, A., Grünwald, T., Heinesch, B., Longdoz, B., Ourcival, J. M., Rambal, S., Vesala, T.,
837   and Dufrêne, E.: Exceptional carbon uptake in European forests during the warm spring of 2007: a data–model
838   analysis, Glob. Chang. Biol., 15, 1455–1474, https://doi.org/10.1111/J.1365-2486.2008.01835.X, 2009.
839

840   Endsley, K. A., Kimball, J. S., Kundig, T., Reichle, R. H., and Ardizzone, J. V: Validation Assessment for the Soil
841   Moisture Active Passive (SMAP) Level 4 Carbon (L4_C) Data Product Version 7, 2023.
842

843   Friedlingstein, P., Cox, P., Betts, R., Bopp, L., von Bloh, W., Brovkin, V., Cadule, P., Doney, S., Eby, M., Fung,
844   I., Bala, G., John, J., Jones, C., Joos, F., Kato, T., Kawamiya, M., Knorr, W., Lindsay, K., Matthews, H. D.,
845   Raddatz, T., Rayner, P., Reick, C., Roeckner, E., Schnitzler, K. G., Schnur, R., Strassmann, K., Weaver, A.

J., Yoshikawa, C., and Zeng, N.: Climate–Carbon Cycle Feedback Analysis: Results from the C4MIP Model Intercomparison, J. Clim., 19, 3337–3353, https://doi.org/10.1175/JCLI3800.1, 2006.

Friedlingstein, P., O'Sullivan, M., Jones, M. W., Andrew, R. M., Bakker, D. C. E., Hauck, J., Landschützer, P., Le Quéré, C., Luijkx, I. T., Peters, G. P., Peters, W., Pongratz, J., Schwingshackl, C., Sitch, S., Canadell, J. G., Ciais, P., Jackson, R. B., Alin, S. R., Anthoni, P., Barbero, L., Bates, N. R., Becker, M., Bellouin, N., Decharme, B., Bopp, L., Brasika, I. B. M., Cadule, P., Chamberlain, M. A., Chandra, N., Chau, T. T. T., Chevallier, F., Chini, L. P., Cronin, M., Dou, X., Enyo, K., Evans, W., Falk, S., Feely, R. A., Feng, L., Ford, D. J., Gasser, T., Ghattas, J., Gkritzalis, T., Grassi, G., Gregor, L., Gruber, N., Gürses, Ö., Harris, I., Hefner, M., Heinke, J., Houghton, R. A., Hurtt, G. C., Iida, Y., Ilyina, T., Jacobson, A. R., Jain, A., Jarníková, T., Jersild, A., Jiang, F., Jin, Z., Joos, F., Kato, E., Keeling, R. F., Kennedy, D., Goldewijk, K. K., Knauer, J., Korsbakken, J. I., Körtzinger, A., Lan, X., Lefèvre, N., Li, H., Liu, J., Liu, Z., Ma, L., Marland, G., Mayot, N., McGuire, P. C., McKinley, G. A., Meyer, G., Morgan, E. J., Munro, D. R., Nakaoka, S. I., Niwa, Y., O'Brien, K. M., Olsen, A., Omar, A. M., Ono, T., Paulsen, M., Pierrot, D., Pocock, K., Poulter, B., Powis, C. M., Rehder, G., Resplandy, L., Robertson, E., Rödenbeck, C., Rosan, T. M., Schwinger, J., Séférian, R., et al.: Global Carbon Budget 2023, Earth Syst. Sci. Data, 15, 5301–5369, https://doi.org/10.5194/ESSD-15-5301-2023, 2023.

Gerten, D., Schaphoff, S., Haberlandt, U., Lucht, W., and Sitch, S.: Terrestrial vegetation and water balance—hydrological evaluation of a dynamic global vegetation model, J. Hydrol., 286, 249–270, https://doi.org/10.1016/J.JHYDROL.2003.09.029, 2004.

Göckede, M., Foken, T., Aubinet, M., Aurela, M., Banza, J., Bernhofer, C., Bonnefond, J. M., Brunet, Y., Carrara, A., Clement, R., Dellwik, E., Elbers, J., Eugster, W., Fuhrer, J., Granier, A., Grünwald, T., Heinesch, B., Janssens, I. A., Knohl, A., Koeble, R., Laurila, T., Longdoz, B., Manca, G., Marek, M., Markkanen, T., Mateus, J., Matteucci, G., Mauder, M., Migliavacca, M., Minerbi, S., Moncrieff, J., Montagnani, L., Moors, E., Ourcival, J. M., Papale, D., Pereira, J., Pilegaard, K., Pita, G., Rambal, S., Rebmann, C., Rodrigues, A., Rotenberg, E., Sanz, M. J., Sedlak, P., Seufert, G., Siebicke, L., Soussana, J. F., Valentini, R., Vesala, T., Verbeeck, H., and Yakir, D.: Quality control of CarboEurope flux data - Part 1: Coupling footprint analyses with flux data quality assessment to evaluate sites in forest ecosystems, Biogeosciences, 5, 433–450, https://doi.org/10.5194/BG-5-433-2008, 2008.

Golaz, J. C., Caldwell, P. M., Van Roekel, L. P., Petersen, M. R., Tang, Q., Wolfe, J. D., Abeshu, G., Anantharaj, V., Asay-Davis, X. S., Bader, D. C., Baldwin, S. A., Bisht, G., Bogenschutz, P. A., Branstetter, M., Brunke, M. A., Brus, S. R., Burrows, S. M., Cameron-Smith, P. J., Donahue, A. S., Deakin, M., Easter, R. C., Evans, K. J., Feng, Y., Flanner, M., Foucar, J. G., Fyke, J. G., Griffin, B. M., Hannay, C., Harrop, B. E., Hoffman, M. J., Hunke, E. C., Jacob, R. L., Jacobsen, D. W., Jeffery, N., Jones, P. W., Keen, N. D., Klein, S. A., Larson, V. E., Leung, L. R., Li, H. Y., Lin, W., Lipscomb, W. H., Ma, P. L., Mahajan, S., Maltrud, M. E., Mametjanov, A., McClean, J. L., McCoy, R. B., Neale, R. B., Price, S. F., Qian, Y., Rasch, P. J., Reeves Eyre, J. E. J., Riley, W. J., Ringler, T. D., Roberts, A. F., Roesler, E. L., Salinger, A. G., Shaheen, Z., Shi, X., Singh, B., Tang, J., Taylor, M. A., Thornton, P. E., Turner, A. K., Veneziani, M., Wan, H., Wang, H., Wang, S., Williams, D. N., Wolfram, P. J., Worley, P. H., Xie, S., Yang, Y., Yoon, J. H., Zelinka, M. D., Zender, C. S., Zeng, X., Zhang, C., Zhang, K., Zhang, Y., Zheng, X., Zhou, T., and Zhu, Q.: The DOE E3SM Coupled Model Version 1: Overview and Evaluation at Standard Resolution, J. Adv. Model. Earth Syst., 11, 2089–2129, https://doi.org/10.1029/2018MS001603, 2019.

Hardouin, L., Delire, C., Decharme, B., Lawrence, D. M., Nabel, J. E. M. S., Brovkin, V., Collier, N., Fisher, R., Hoffman, F. M., Koven, C. D., Séférian, R., and Stacke, T.: Uncertainty in land carbon budget simulated by terrestrial biosphere models: the role of atmospheric forcing, Environ. Res. Lett., 17, 094033, https://doi.org/10.1088/1748-9326/AC888D, 2022.

Haszpra, L., Barcza, Z., Davis, K. J., and Tarczay, K.: Long-term tall tower carbon dioxide flux monitoring over an area of mixed vegetation, Agric. For. Meteorol., 132, 58–77, https://doi.org/10.1016/J.AGRFORMET.2005.07.002, 2005.

Haverd, V., Smith, B., Nieradzik, L., Briggs, P. R., Woodgate, W., Trudinger, C. M., Canadell, J. G., and Cuntz, M.: A new version of the CABLE land surface model (Subversion revision r4601) incorporating land use and land cover change, woody vegetation demography, and a novel optimisation-based approach to plant coordination of photosynthesis, Geosci. Model Dev., 11, 2995–3026, https://doi.org/10.5194/GMD-11-2995-2018, 2018.

He, B., Chen, C., Lin, S., Yuan, W., Chen, H. W., Chen, D., Zhang, Y., Guo, L., Zhao, X., Liu, X., Piao, S., Zhong, Z., Wang, R., and Tang, R.: Worldwide impacts of atmospheric vapor pressure deficit on the interannual variability of terrestrial carbon sinks, Natl. Sci. Rev., 9, nwab150, https://doi.org/10.1093/NSR/NWAB150, 2022.

Hersbach, H., Bell, B., Berrisford, P., Hirahara, S., Horányi, A., Muñoz-Sabater, J., Nicolas, J., Peubey, C., Radu, R., Schepers, D., Simmons, A., Soci, C., Abdalla, S., Abellan, X., Balsamo, G., Bechtold, P., Biavati, G., Bidlot, J., Bonavita, M., De Chiara, G., Dahlgren, P., Dee, D., Diamantakis, M., Dragani, R., Flemming, J., Forbes, R., Fuentes, M., Geer, A., Haimberger, L., Healy, S., Hogan, R. J., Hólm, E., Janisková, M., Keeley, S., Laloyaux, P., Lopez, P., Lupu, C., Radnoti, G., de Rosnay, P., Rozum, I., Vamborg, F., Villaume, S., and Thépaut, J. N.: The ERA5 global reanalysis, Q. J. R. Meteorol. Soc., 146, 1999–2049, https://doi.org/10.1002/QJ.3803, 2020.

Jinxun, L., Xuehe, L., Qiuan, Z., Wenping, Y., Quanzhi, Y., Zhen, Z., Qingxi, G., Carol, D., Jinxun, L., Xuehe, L., Qiuan, Z., Wenping, Y., Quanzhi, Y., Zhen, Z., Qingxi, G., and Carol, D.: Terrestrial Ecosystem Modeling with IBIS: Progress and Future Vision, J. Resour. Ecol., 13, 2–16, https://doi.org/10.5814/J.ISSN.1674-764X.2022.01.001, 2022.

Jones, L. A., Kimball, J. S., Reichle, R. H., Madani, N., Glassy, J., Ardizzone, J. V., Colliander, A., Cleverly, J., Desai, A. R., Eamus, D., Euskirchen, E. S., Hutley, L., Macfarlane, C., and Scott, R. L.: The SMAP Level 4 Carbon Product for Monitoring Ecosystem Land-Atmosphere CO2 Exchange, IEEE Trans. Geosci. Remote Sens., 55, 6517–6532, https://doi.org/10.1109/TGRS.2017.2729343, 2017.

Jung, M., Koirala, S., Weber, U., Ichii, K., Gans, F., Camps-Valls, G., Papale, D., Schwalm, C., Tramontana, G., and Reichstein, M.: The FLUXCOM ensemble of global land-atmosphere energy fluxes, Sci. Data 2019 61, 6, 1–14, https://doi.org/10.1038/s41597-019-0076-8, 2019.

Jung, M., Schwalm, C., Migliavacca, M., Walther, S., Camps-Valls, G., Koirala, S., Anthoni, P., Besnard, S., Bodesheim, P., Carvalhais, N., Chevallier, F., Gans, F., S Goll, D., Haverd, V., Köhler, P., Ichii, K., K Jain, A., Liu, J., Lombardozzi, D., E M S Nabel, J., A Nelson, J., O'Sullivan, M., Pallandt, M., Papale, D., Peters, W., Pongratz, J., Rödenbeck, C., Sitch, S., Tramontana, G., Walker, A., Weber, U., and Reichstein, M.: Scaling carbon fluxes from eddy covariance sites to globe: Synthesis and evaluation of the FLUXCOM approach, Biogeosciences, 17, 1343–1365, https://doi.org/10.5194/BG-17-1343-2020, 2020.

Kimball, J. S., Endsley, K. A., Jones, L. A., Kundig, T., and Reichle, R.: SMAP L4 Global Daily 9 km EASE-Grid Carbon Net Ecosystem Exchange, Version 7 | National Snow and Ice Data Center, https://doi.org/https://doi.org/10.5067/3K9F0S1Q5J2U., 2022.

Kong, Z., Wang, T., Han, Q., Dai, Y., Wang, L., and Chen, X.: Evaluation of Environmental Controls on Terrestrial Net Ecosystem Exchange of CO2: A Global Perspective From the FLUXNET Sites, J. Geophys. Res. Atmos., 127, e2022JD037217, https://doi.org/10.1029/2022JD037217, 2022.

Krinner, G., Viovy, N., de Noblet-Ducoudré, N., Ogée, J., Polcher, J., Friedlingstein, P., Ciais, P., Sitch, S., and Prentice, I. C.: A dynamic global vegetation model for studies of the coupled atmosphere-biosphere system, Global Biogeochem. Cycles, 19, 1–33, https://doi.org/10.1029/2003GB002199, 2005.

Kurbatova, J., Li, C., Varlagin, A., Xiao, X., and Vygodskaya, N.: Modeling carbon dynamics in two adjacent spruce forests with different soil conditions in Russia, Biogeosciences, 5, 969–980, https://doi.org/10.5194/BG-5-969-2008, 2008.

Lasslop, G., Reichstein, M., Papale, D., Richardson, A., Arneth, A., Barr, A., Stoy, P., and Wohlfahrt, G.: Separation of net ecosystem exchange into assimilation and respiration using a light response curve approach: critical issues and global evaluation, Glob. Chang. Biol., 16, 187–208, https://doi.org/10.1111/J.1365-2486.2009.02041.X, 2010.

Lawrence, D. M., Fisher, R. A., Koven, C. D., Oleson, K. W., Swenson, S. C., Bonan, G., Collier, N., Ghimire, B., van Kampenhout, L., Kennedy, D., Kluzek, E., Lawrence, P. J., Li, F., Li, H., Lombardozzi, D., Riley, W. J., Sacks, W. J., Shi, M., Vertenstein, M., Wieder, W. R., Xu, C., Ali, A. A., Badger, A. M., Bisht, G., van den Broeke, M., Brunke, M. A., Burns, S. P., Buzan, J., Clark, M., Craig, A., Dahlin, K., Drewniak, B., Fisher,

J. B., Flanner, M., Fox, A. M., Gentine, P., Hoffman, F., Keppel-Aleks, G., Knox, R., Kumar, S., Lenaerts, J., Leung, L. R., Lipscomb, W. H., Lu, Y., Pandey, A., Pelletier, J. D., Perket, J., Randerson, J. T., Ricciuto, D. M., Sanderson, B. M., Slater, A., Subin, Z. M., Tang, J., Thomas, R. Q., Val Martin, M., and Zeng, X.: The Community Land Model Version 5: Description of New Features, Benchmarking, and Impact of Forcing Uncertainty, J. Adv. Model. Earth Syst., 11, 4245–4287, https://doi.org/10.1029/2018MS001583, 2019.

Le Quéré, C., Andrew, R. M., Friedlingstein, P., Sitch, S., Pongratz, J., Manning, A. C., Korsbakken, J. I., Peters, G. P., Canadell, J. G., Jackson, R. B., Boden, T. A., Tans, P. P., Andrews, O. D., Arora, V. K., Bakker, D. C. E., Barbero, L., Becker, M., Betts, R. A., Bopp, L., Chevallier, F., Chini, L. P., Ciais, P., Cosca, C. E., Cross, J., Currie, K., Gasser, T., Harris, I., Hauck, J., Haverd, V., Houghton, R. A., Hunt, C. W., Hurtt, G., Ilyina, T., Jain, A. K., Kato, E., Kautz, M., Keeling, R. F., Klein Goldewijk, K., Körtzinger, A., Landschützer, P., Lefèvre, N., Lenton, A., Lienert, S., Lima, I., Lombardozzi, D., Metzl, N., Millero, F., Monteiro, P. M. S., Munro, D. R., Nabel, J. E. M. S., Nakaoka, S., Nojiri, Y., Padin, X. A., Peregon, A., Pfeil, B., Pierrot, D., Poulter, B., Rehder, G., Reimer, J., Rödenbeck, C., Schwinger, J., Séférian, R., Skjelvan, I., Stocker, B. D., Tian, H., Tilbrook, B., Tubiello, F. N., van der Laan-Luijkx, I. T., van der Werf, G. R., van Heuven, S., Viovy, N., Vuichard, N., Walker, A. P., Watson, A. J., Wiltshire, A. J., Zaehle, S., and Zhu, D.: Global Carbon Budget 2017, Earth Syst. Sci. Data, 10, 405–448, https://doi.org/10.5194/essd-10-405-2018, 2018.

Li, Q., Tietema, A., Reinsch, S., Schmidt, I. K., de Dato, G., Guidolotti, G., Lellei-Kovács, E., Kopittke, G., and Larsen, K. S.: Higher sensitivity of gross primary productivity than ecosystem respiration to experimental drought and warming across six European shrubland ecosystems, Sci. Total Environ., 900, 165627, https://doi.org/10.1016/j.scitotenv.2023.165627, 2023.

Lienert, S. and Joos, F.: A Bayesian ensemble data assimilation to constrain model parameters and land-use carbon emissions, Biogeosciences, 15, 2909–2930, https://doi.org/10.5194/BG-15-2909-2018, 2018.

Lin, S., Hu, Z., Wang, Y., Chen, X., He, B., Song, Z., Sun, S., Wu, C., Zheng, Y., Xia, X., Liu, L., Tang, J., Sun, Q., Joos, F., and Yuan, W.: Underestimated Interannual Variability of Terrestrial Vegetation Production by Terrestrial Ecosystem Models, Global Biogeochem. Cycles, 37, e2023GB007696, https://doi.org/10.1029/2023GB007696, 2023.

Lindeskog, M., Smith, B., Lagergren, F., Sycheva, E., Ficko, A., Pretzsch, H., and Rammig, A.: Accounting for forest management in the estimation of forest carbon balance using the dynamic vegetation model LPJ-GUESS (v4.0, r9710): Implementation and evaluation of simulations for Europe, 6071–6112 pp., https://doi.org/10.5194/gmd-14-6071-2021, 2021.

Longo, M., Knox, R. G., Medvigy, D. M., Levine, N. M., Dietze, M. C., Kim, Y., Swann, A. L. S., Zhang, K., Rollinson, C. R., Bras, R. L., Wofsy, S. C., and Moorcroft, P. R.: The biophysics, ecology, and biogeochemistry of functionally diverse, vertically and horizontally heterogeneous ecosystems: The Ecosystem Demography model, version 2.2-Part 1: Model description, Geosci. Model Dev., 12, 4309–4346, https://doi.org/10.5194/GMD-12-4309-2019, 2019.

Madani, N., Kimball, J. S., Jones, L. A., Parazoo, N. C., and Guan, K.: Global Analysis of Bioclimatic Controls on Ecosystem Productivity Using Satellite Observations of Solar-Induced Chlorophyll Fluorescence, Remote Sens. 2017, Vol. 9, Page 530, 9, 530, https://doi.org/10.3390/RS9060530, 2017.

Martinez del Castillo, E., Zang, C. S., Buras, A., Hacket-Pain, A., Esper, J., Serrano-Notivoli, R., Hartl, C., Weigel, R., Klesse, S., Resco de Dios, V., Scharnweber, T., Dorado-Liñán, I., van der Maaten-Theunissen, M., van der Maaten, E., Jump, A., Mikac, S., Banzragch, B. E., Beck, W., Cavin, L., Claessens, H., Čada, V., Čufar, K., Dulamsuren, C., Gričar, J., Gil-Pelegrín, E., Janda, P., Kazimirovic, M., Kreyling, J., Latte, N., Leuschner, C., Longares, L. A., Menzel, A., Merela, M., Motta, R., Muffler, L., Nola, P., Petritan, A. M., Petritan, I. C., Prislan, P., Rubio-Cuadrado, Á., Rydval, M., Stajić, B., Svoboda, M., Toromani, E., Trotsiuk, V., Wilmking, M., Zlatanov, T., and de Luis, M.: Climate-change-driven growth decline of European beech forests, Commun. Biol. 2022 51, 5, 1–9, https://doi.org/10.1038/s42003-022-03107-3, 2022.

Messori, G., Ruiz-Pérez, G., Manzoni, S., and Vico, G.: Climate drivers of the terrestrial carbon cycle variability in Europe, Environ. Res. Lett., 14, 063001, https://doi.org/10.1088/1748-9326/AB1AC0, 2019.

Monteith, J. and Unsworth, M.: Principles of Environmental Physics - 3rd Edition, Academic Press, 440 pp., 2007.

1025
1026 Muñoz Sabater, J.: ERA5-Land hourly data from 1950 to present. Copernicus Climate Change Service (C3S)
1027   Climate Data Store (CDS), https://doi.org/10.24381/cds.e2161bac, 2019.
1028
1029 Nelson, J. A., Walther, S., Gans, F., Kraft, B., Weber, U., Novick, K., Buchmann, N., Migliavacca, M., Wohlfahrt,
1030   G., Šigut, L., Ibrom, A., Papale, D., Göckede, M., Duveiller, G., Knohl, A., Hörtnagl, L., Scott, R. L., Dušek,
1031   J., Zhang, W., Hamdi, Z. M., Reichstein, M., Aranda-Barranco, S., Ardö, J., Op de Beeck, M., Billesbach, D.,
1032   Bowling, D., Bracho, R., Brümmer, C., Camps-Valls, G., Chen, S., Cleverly, J. R., Desai, A., Dong, G., El-
1033   Madany, T. S., Euskirchen, E. S., Feigenwinter, I., Galvagno, M., Gerosa, G. A., Gielen, B., Goded, I., Goslee,
1034   S., Gough, C. M., Heinesch, B., Ichii, K., Jackowicz-Korczynski, M. A., Klosterhalfen, A., Knox, S.,
1035   Kobayashi, H., Kohonen, K.-M., Korkiakoski, M., Mammarella, I., Gharun, M., Marzuoli, R., Matamala, R.,
1036   Metzger, S., Montagnani, L., Nicolini, G., O'Halloran, T., Ourcival, J.-M., Peichl, M., Pendall, E., Ruiz
1037   Reverter, B., Roland, M., Sabbatini, S., Sachs, T., Schmidt, M., Schwalm, C. R., Shekhar, A., Silberstein, R.,
1038   Silveira, M. L., Spano, D., Tagesson, T., Tramontana, G., Trotta, C., Turco, F., Vesala, T., Vincke, C., Vitale,
1039   D., Vivoni, E. R., Wang, Y., Woodgate, W., Yepez, E. A., Zhang, J., Zona, D., and Jung, M.: X-BASE: the
1040   first terrestrial carbon and water flux products from an extended data-driven scaling framework, FLUXCOM-
1041   X, Biogeosciences, 21, 5079–5115, https://doi.org/10.5194/BG-21-5079-2024, 2024.
1042
1043 Pan, Y., Birdsey, R. A., Phillips, O. L., Houghton, R. A., Fang, J., Kauppi, P. E., Keith, H., Kurz, W. A., Ito, A.,
1044   Lewis, S. L., Nabuurs, G.-J., Shvidenko, A., Hashimoto, S., Lerink, B., Schepaschenko, D., Castanho, A., and
1045   Murdiyarso, D.: The enduring world forest carbon sink, Nature, 631, 563–569,
1046   https://doi.org/10.1038/s41586-024-07602-x, 2024.
1047
1048 Pastorello, G., Trotta, C., Canfora, E., Chu, H., Christianson, D., Cheah, Y. W., Poindexter, C., Chen, J.,
1049   Elbashandy, A., Humphrey, M., Isaac, P., Polidori, D., Ribeca, A., van Ingen, C., Zhang, L., Amiro, B.,
1050   Ammann, C., Arain, M. A., Ardö, J., Arkebauer, T., Arndt, S. K., Arriga, N., Aubinet, M., Aurela, M.,
1051   Baldocchi, D., Barr, A., Beamesderfer, E., Marchesini, L. B., Bergeron, O., Beringer, J., Bernhofer, C.,
1052   Berveiller, D., Billesbach, D., Black, T. A., Blanken, P. D., Bohrer, G., Boike, J., Bolstad, P. V., Bonal, D.,
1053   Bonnefond, J. M., Bowling, D. R., Bracho, R., Brodeur, J., Brümmer, C., Buchmann, N., Burban, B., Burns,
1054   S. P., Buysse, P., Cale, P., Cavagna, M., Cellier, P., Chen, S., Chini, I., Christensen, T. R., Cleverly, J., Collalti,
1055   A., Consalvo, C., Cook, B. D., Cook, D., Coursolle, C., Cremonese, E., Curtis, P. S., D'Andrea, E., da Rocha,
1056   H., Dai, X., Davis, K. J., De Cinti, B., de Grandcourt, A., De Ligne, A., De Oliveira, R. C., Delpierre, N.,
1057   Desai, A. R., Di Bella, C. M., di Tommasi, P., Dolman, H., Domingo, F., Dong, G., Dore, S., Duce, P.,
1058   Dufrêne, E., Dunn, A., Dušek, J., Eamus, D., Eichelmann, U., ElKhidir, H. A. M., Eugster, W., Ewenz, C. M.,
1059   Ewers, B., Famulari, D., Fares, S., Feigenwinter, I., Feitz, A., Fensholt, R., Filippa, G., Fischer, M., Frank, J.,
1060   Galvagno, M., Gharun, M., Gianelle, D., et al.: The FLUXNET2015 dataset and the ONEFlux processing
1061   pipeline for eddy covariance data, Sci. Data 2020 71, 7, 1–27, https://doi.org/10.1038/s41597-020-0534-3,
1062   2020.
1063
1064 Piao, S., Ciais, P., Friedlingstein, P., De Noblet-Ducoudré, N., Cadule, P., Viovy, N., and Wang, T.:
1065   Spatiotemporal patterns of terrestrial carbon cycle during the 20th century, Global Biogeochem. Cycles, 23,
1066   https://doi.org/10.1029/2008GB003339, 2009.
1067
1068 Prentice, I. C., Farquhar, G. D., Fasham, M. J. R., Goulden, M. L., Heimann, M., Jaramillo, V. J., Kheshgi, H. S.,
1069   Le Quéré, C., Scholes, R. J., Contributing, D. W. R. W., Archer, D., Ashmore, M. R., Aumont, O., Baker, D.,
1070   Battle, M., Bender, M., Bopp, L. P., Bousquet, P., Caldeira, K., Ciais, P., Cox, P. M., Cramer, W., Dentener,
1071   F., Enting, I. G., Field, C. B., Friedlingstein, P., Holland, E. A., Houghton, R. A., House, J. I., Ishida, A., Jain,
1072   A. K., Janssens, I. A., Joos, F., Kaminski, T., Keeling, C. D., Keeling, R. F., Kicklighter, D. W., Kohfeld, K.
1073   E., Knorr, W., Law, R., Lenton, T., Lindsay, K., Maier-Reimer, E., Manning, A. C., Matear, R. J., Mcguire,
1074   A. D., Melillo, J. M., Meyer, R., Mund, M., Orr, J. C., Piper, S., Plattner, K., Rayner, P. J., Sitch, S., Slater,
1075   R., Taguchi, S., Tans, P. P., Tian, H. Q., Weirig, M. F., Whorf, T., Review, A. Y., Pitelka, E. L., and Rojas,
1076   A. R.: The Carbon Cycle and Atmospheric Carbon Dioxide, in Climate Change 2001: The Scientific Basis.
1077   Contribution of Working Group I to the Third Assessment Report of the Intergovernmental Panel on Climate
1078   Change, 183–237 pp., 2001.
1079
1080 Pugh, T. A. M., Lindeskog, M., Smith, B., Poulter, B., Arneth, A., Haverd, V., and Calle, L.: Role of forest
1081   regrowth in global carbon sink dynamics, Proc. Natl. Acad. Sci. U. S. A., 116, 4382–4387,
1082   https://doi.org/10.1073/PNAS.1810512116/SUPPL_FILE/PNAS.1810512116.SD02.TXT, 2019.
1083
1084 Saunders, M., Tobin, B., Black, K., Gioria, M., Nieuwenhuis, M., and Osborne, B. A.: Thinning effects on the net

ecosystem carbon exchange of a Sitka spruce forest are temperature-dependent, Agric. For. Meteorol., 157, 1–10, https://doi.org/10.1016/J.AGRFORMET.2012.01.008, 2012.

Schimel, D., Stephens, B. B., and Fisher, J. B.: Effect of increasing CO2 on the terrestrial carbon cycle, Proc. Natl. Acad. Sci. U. S. A., 112, 436–441, https://doi.org/10.1073/PNAS.1407302112/SUPPL_FILE/PNAS.201407302SI.PDF, 2015.

Seddon, A. W. R., Macias-Fauria, M., Long, P. R., Benz, D., and Willis, K. J.: Sensitivity of global terrestrial ecosystems to climate variability, Nat. 2016 5317593, 531, 229–232, https://doi.org/10.1038/nature16986, 2016.

Seiler, C., Melton, J. R., Arora, V. K., and Wang, L.: CLASSIC v1.0: The open-source community successor to the Canadian Land Surface Scheme (CLASS) and the Canadian Terrestrial Ecosystem Model (CTEM) - Part 2: Global benchmarking, Geosci. Model Dev., 14, 2371–2417, https://doi.org/10.5194/GMD-14-2371-2021, 2021.

Sharma, B., Kumar, J., Collier, N., Ganguly, A. R., and Hoffman, F. M.: Quantifying Carbon Cycle Extremes and Attributing Their Causes Under Climate and Land Use and Land Cover Change From 1850 to 2300, J. Geophys. Res. Biogeosciences, 127, e2021JG006738, https://doi.org/10.1029/2021JG006738, 2022.

Sitch, S., Huntingford, C., Gedney, N., Levy, P. E., Lomas, M., Piao, S. L., Betts, R., Ciais, P., Cox, P., Friedlingstein, P., Jones, C. D., Prentice, I. C., and Woodward, F. I.: Evaluation of the terrestrial carbon cycle, future plant geography and climate-carbon cycle feedbacks using five Dynamic Global Vegetation Models (DGVMs), Glob. Chang. Biol., 14, 2015–2039, https://doi.org/10.1111/J.1365-2486.2008.01626.X, 2008.

Sitch, S., O'Sullivan, M., Robertson, E., Friedlingstein, P., Albergel, C., Anthoni, P., Arneth, A., Arora, V. K., Bastos, A., Bastrikov, V., Bellouin, N., Canadell, J. G., Chini, L., Ciais, P., Falk, S., Harris, I., Hurtt, G., Ito, A., Jain, A. K., Jones, M. W., Joos, F., Kato, E., Kennedy, D., Klein Goldewijk, K., Kluzek, E., Knauer, J., Lawrence, P. J., Lombardozzi, D., Melton, J. R., Nabel, J. E. M. S., Pan, N., Peylin, P., Pongratz, J., Poulter, B., Rosan, T. M., Sun, Q., Tian, H., Walker, A. P., Weber, U., Yuan, W., Yue, X., and Zaehle, S.: Trends and Drivers of Terrestrial Sources and Sinks of Carbon Dioxide: An Overview of the TRENDY Project, Global Biogeochem. Cycles, 38, e2024GB008102, https://doi.org/10.1029/2024GB008102, 2024.

Smith, N. E., Kooijmans, L. M. J., Koren, G., Van Schaik, E., Van Der Woude, A. M., Wanders, N., Ramonet, M., Xueref-Remy, I., Siebicke, L., Manca, G., Brümmer, C., Baker, I. T., Haynes, K. D., Luijkx, I. T., and Peters, W.: Spring enhancement and summer reduction in carbon uptake during the 2018 drought in northwestern Europe, Philos. Trans. R. Soc. B, 375, https://doi.org/10.1098/RSTB.2019.0509, 2020.

Tang, X., Li, H., Desai, A. R., Nagy, Z., Luo, J., Kolb, T. E., Olioso, A., Xu, X., Yao, L., Kutsch, W., Pilegaard, K., Köstner, B., and Ammann, C.: How is water-use efficiency of terrestrial ecosystems distributed and changing on Earth?, Sci. Reports 2014 41, 4, 1–11, https://doi.org/10.1038/srep07483, 2014.

Team, W. W., and Centre, I. E. T.: Warm Winter 2020 ecosystem eddy covariance flux product for 73 stations in FLUXNET-Archive format—release 2022-1, https://doi.org/https://doi.org/10.18160/2G60-ZHAK, 2022.

Thompson, R. L., Broquet, G., Gerbig, C., Koch, T., Lang, M., Monteil, G., Munassar, S., Nickless, A., Scholze, M., Ramonet, M., Karstens, U., Van Schaik, E., Wu, Z., and Rödenbeck, C.: Changes in net ecosystem exchange over Europe during the 2018 drought based on atmospheric observations, Philos. Trans. R. Soc. B, 375, https://doi.org/10.1098/RSTB.2019.0512, 2020.

Tian, H., Lu, C., Ciais, P., Michalak, A. M., Canadell, J. G., Saikawa, E., Huntzinger, D. N., Gurney, K. R., Sitch, S., Zhang, B., Yang, J., Bousquet, P., Bruhwiler, L., Chen, G., Dlugokencky, E., Friedlingstein, P., Melillo, J., Pan, S., Poulter, B., Prinn, R., Saunois, M., Schwalm, C. R., and Wofsy, S. C.: The terrestrial biosphere as a net source of greenhouse gases to the atmosphere, Nat. 2016 5317593, 531, 225–228, https://doi.org/10.1038/nature16946, 2016.

Tramontana, G., Jung, M., Schwalm, C. R., Ichii, K., Camps-Valls, G., Ráduly, B., Reichstein, M., Arain, M. A., Cescatti, A., Kiely, G., Merbold, L., Serrano-Ortiz, P., Sickert, S., Wolf, S., and Papale, D.: Predicting carbon dioxide and energy fluxes across global FLUXNET sites with regression algorithms, Biogeosciences, 13, 4291–4313, https://doi.org/10.5194/BG-13-4291-2016, 2016.

Valentini, R., Arneth, A., Bombelli, A., Castaldi, S., Cazzolla Gatti, R., Chevallier, F., Ciais, P., Grieco, E., Hartmann, J., Henry, M., Houghton, R. A., Jung, M., Kutsch, W. L., Malhi, Y., Mayorga, E., Merbold, L., Murray-Tortarolo, G., Papale, D., Peylin, P., Poulter, B., Raymond, P. A., Santini, M., Sitch, S., Vaglio Laurin, G., Van Der Werf, G. R., Williams, C. A., and Scholes, R. J.: A full greenhouse gases budget of africa: Synthesis, uncertainties, and vulnerabilities, Biogeosciences, 11, 381–407, https://doi.org/10.5194/BG-11-381-2014, 2014.

van der Woude, A. M., Peters, W., Joetzjer, E., Lafont, S., Koren, G., Ciais, P., Ramonet, M., Xu, Y., Bastos, A., Botía, S., Sitch, S., de Kok, R., Kneuer, T., Kubistin, D., Jacotot, A., Loubet, B., Herig-Coimbra, P. H., Loustau, D., and Luijkx, I. T.: Temperature extremes of 2022 reduced carbon uptake by forests in Europe, Nat. Commun. 2023 141, 14, 1–11, https://doi.org/10.1038/s41467-023-41851-0, 2023.

von Buttlar, J., Zscheischler, J., Rammig, A., Sippel, S., Reichstein, M., Knohl, A., Jung, M., Menzer, O., Arain, M. A., Buchmann, N., Cescatti, A., Gianelle, D., Kiely, G., Law, B. E., Magliulo, V., Margolis, H., McCaughey, H., Merbold, L., Migliavacca, M., Montagnani, L., Oechel, W., Pavelka, M., Peichl, M., Rambal, S., Raschi, A., Scott, R. L., Vaccari, F. P., Van Gorsel, E., Varlagin, A., Wohlfahrt, G., and Mahecha, M. D.: Impacts of droughts and extreme-temperature events on gross primary production and ecosystem respiration: a systematic assessment across ecosystems and climate zones, Biogeosciences, 15, 1293–1318, https://doi.org/10.5194/bg-15-1293-2018, 2018.

Walker, A. P., De Kauwe, M. G., Bastos, A., Belmecheri, S., Georgiou, K., Keeling, R. F., McMahon, S. M., Medlyn, B. E., Moore, D. J. P., Norby, R. J., Zaehle, S., Anderson-Teixeira, K. J., Battipaglia, G., Brienen, R. J. W., Cabugao, K. G., Cailleret, M., Campbell, E., Canadell, J. G., Ciais, P., Craig, M. E., Ellsworth, D. S., Farquhar, G. D., Fatichi, S., Fisher, J. B., Frank, D. C., Graven, H., Gu, L., Haverd, V., Heilman, K., Heimann, M., Hungate, B. A., Iversen, C. M., Joos, F., Jiang, M., Keenan, T. F., Knauer, J., Körner, C., Leshyk, V. O., Leuzinger, S., Liu, Y., MacBean, N., Malhi, Y., McVicar, T. R., Penuelas, J., Pongratz, J., Powell, A. S., Riutta, T., Sabot, M. E. B., Schleucher, J., Sitch, S., Smith, W. K., Sulman, B., Taylor, B., Terrer, C., Torn, M. S., Treseder, K. K., Trugman, A. T., Trumbore, S. E., van Mantgem, P. J., Voelker, S. L., Whelan, M. E., and Zuidema, P. A.: Integrating the evidence for a terrestrial carbon sink caused by increasing atmospheric CO2, New Phytol., 229, 2413–2445, https://doi.org/10.1111/NPH.16866, 2021.

Wang, J., Chen, J., Zhang, J., Yang, S., Zhang, S., Bai, Y., and Xu, R.: Consistency and uncertainty of remote sensing-based approaches for regional yield gap estimation: A comprehensive assessment of process-based and data-driven models, F. Crop. Res., 302, 109088, https://doi.org/10.1016/J.FCR.2023.109088, 2023.

Welp, L. R., Randerson, J. T., and Liu, H. P.: The sensitivity of carbon fluxes to spring warming and summer drought depends on plant functional type in boreal forest ecosystems, Agric. For. Meteorol., 147, 172–185, https://doi.org/10.1016/J.AGRFORMET.2007.07.010, 2007.

Woodward, F. I. and Lomas, M. R.: Vegetation dynamics--simulating responses to climatic change, Biol. Rev. Camb. Philos. Soc., 79, 643–670, https://doi.org/10.1017/S1464793103006419, 2004.

Wu, Z., Ahlström, A., Smith, B., Ardö, J., Eklundh, L., Fensholt, R., and Lehsten, V.: Climate data induced uncertainty in model-based estimations of terrestrial primary productivity, Environ. Res. Lett., 12, 064013, https://doi.org/10.1088/1748-9326/AA6FD8, 2017.

Xia, J., Chen, Y., Liang, S., Liu, D., and Yuan, W.: Global simulations of carbon allocation coefficients for deciduous vegetation types, Tellus B Chem. Phys. Meteorol., 6, https://doi.org/10.3402/TELLUSB.V67.28016, 2015.

Xu, S., Gentine, P., Li, L., Wang, L., Yu, Z., Dong, N., Ju, Q., and Zhang, Y.: Response of Ecosystem Productivity to High Vapor Pressure Deficit and Low Soil Moisture: Lessons Learned From the Global Eddy-Covariance Observations, Earth's Futur., 11, e2022EF003252, https://doi.org/10.1029/2022EF003252, 2023.

Zaehle, S., Friend, A. D., Friedlingstein, P., Dentener, F., Peylin, P., and Schulz, M.: Carbon and nitrogen cycle dynamics in the O-CN land surface model: 2. Role of the nitrogen cycle in the historical terrestrial carbon balance, Global Biogeochem. Cycles, 24, 1006, https://doi.org/10.1029/2009GB003522, 2010.

Zhuravlev, R., Dara, A., Santos, A. L. D. dos, Demidov, O., and Burba, G.: Globally Scalable Approach to

1205   Estimate Net Ecosystem Exchange Based on Remote Sensing, Meteorological Data, and Direct Measurements
1206   of Eddy Covariance Sites, Remote Sens. 2022, Vol. 14, Page 5529, 14, 5529,
1207   https://doi.org/10.3390/RS14215529, 2022.
1208
1209